5-2010

Newly-Developed Nanostructured Microcantilever Arrays for Gas-phase and Liquid-phase Sensing

Zhou Long
UT, Knoxville, zlong@utk.edu

To the Graduate Council:

I am submitting herewith a dissertation written by Zhou Long entitled "Newly-Developed Nanostructured Microcantilever Arrays for Gas-phase and Liquid-phase Sensing." I have examined the final electronic copy of this dissertation for form and content and recommend that it be accepted in partial fulfillment of the requirements for the degree of Doctor of Philosophy, with a major in Chemistry.

Michael J. Sepaniak, Major Professor

We have read this dissertation and recommend its acceptance:

Frank Vogt, Ziling Xue, Panos Datskos

Accepted for the Council:

Carolyn R. Hodges

Vice Provost and Dean of the Graduate School

(Original signatures are on file with official student records.)

To the Graduate Council:

I am submitting herewith a dissertation written by Zhou Long entitled "Newly-Developed Nanostructured Microcantilever Arrays for Gas-phase and Liquid-phase Sensing." I have examined the final electronic copy of this dissertation for form and content and recommend that it be accepted in partial fulfillment of the requirements for the degree of Doctor of Philosophy, with a major in Chemistry.

Dr. Michael Sepaniak, Major Professor

We have read this dissertation
and recommend its acceptance:

Dr. Panos Datskos

Dr. Ziling Xue

Dr. Frank Vogt

Acceptance for the Council:

Carolyn R. Hodges
Vice Provost and Dean of the Graduate School

(Original signatures are on file with official student records.)

NEWLY-DEVELOPED NANOSTRUCTURED MICROCANTILEVER ARRAYS FOR GAS-PHASE AND LIQUID-PHASE SENSING

A Dissertation
Presented for the
Doctor of Philosophy Degree
The University of Tennessee, Knoxville

Zhou Long

May 2010

ACKNOWLEDMENTS

I would like to take this opportunity to thank all the people who helped me with this work and with my graduate study.

I would like to thank my family: my wife Cindy who always supports my career, and my parents who give me encouragement and comfort all the time.

I would like to thank Dr. Sepaniak who consistently gave me academic and research advice through my graduate career at the University of Tennessee, which made me become more professional with a lot of new expertise as a chemist. Dr. Peter Chapman helped me to learn about microcantilever sensors and with my personal life. I would also like to give special thanks to the friends I have met and worked with during my graduate study in Dr. Sepaniak's group, Dr. Maggie Connatser, Dr. Pampa Dutta, Dr. Kathleen Giesfeldt, Dr. Nahla AbuHatab, Dr. Marco DeJesus, Dr. Jenny Oran, Dr. Amber Wellman, Dr. Lance Riddle, Kasey Hill, Matt Walworth, Deepak Bhandari, Sabrina Wells, Lisa Taylor, Jim Patton, and Joshy John. Your help in my research work and the comfortable environment you guys have created made a productive and joyful period of 5 years in this group. I would also thank Dr. Panos Datskos, Mr. Sam Lewis, Mr. John Storey and Dr. Gerald DeVault for offering me opportunities to collaborate with other researchers outside the University of Tennessee.

I would also like to thank Department of Chemistry, University of Tennessee for providing financial support to enable me to finish this research work.

I would also like to thank Tim Free and Gary Wynn who gave support on experimental instrument, and Bill Gurley who offered support on computers.

Finally, I would like to thank my committee members: Dr. Vogt, Dr. Datskos, and Dr. Xue. Thank you very much for your willingness to serve on my committee.

ABSTRACT

The microcantilever (MC) has become a common transducer for chemical and biological sensing in gas phase and liquid phase during recent years. MC sensors provide superior mass sensitivity by converting weak chemical and biological stimuli into high mechanical response. Moreover, other advantages such as small size, low cost and array format have made MCs more attractive than other comparable sensors.

Selectivity in MC sensors can be enhanced by creating a differentially functionalized MC array (MCA) with responsive phases (RPs). A well-designed array should incorporate RPs exhibiting a variety of possible interactions with the analytes, and a specific analyte should induce a distinctive response pattern demonstrated by the array.

The first major division of the dissertation research work focused on enhancing selectivity of MC sensor by creating a differentiating MCA. The MCs within the array were nanostructured in a previously developed manner. A self-designed capillary array was set up to chemically functionalize different ligands onto individual MCs in an array for metal ion sensing in liquid phase. Another array was prepared by selectively vapor depositing different organic RPs onto nanostructured MCs and applied to landfill siloxane sensing in gas phase. Both of the arrays demonstrated response diversity to the target analytes.

The second major division of the dissertation research work focused on developing a new method to modify MC surfaces with a function nanostructure. Aluminium oxide nanoparticles (AONP) were uniformly dispersed onto MC and a

roughened surface with high surface area was achieved as stable sensor platform. Alkoxysilyl compounds were then grafted onto this platform as RPs. For demonstration, a MCA functionalized with three different alkoxysilanes was prepared for volatile organic compound sensing in gas phase. Additionally, another MCA was functionalized with anti-human immunoglobulin G and anti-biotin for bio-sensing in liquid phase. Both of the arrays were prepared with the aforementioned capillary array setup. Selective responses of specific analytes, as well as good sensitivity, were obtained from each type of AONP MCA.

TABLE OF CONTENTS

LIST OF Figures

LIST OF TABLES

ABBREVIATIONS AND SYMBOLS

AcβCD: heptakis(6-O-tert-butyldimethylsilyl-2,3-di-O-acetyl)-β-cyclodextrin

AET: 2-aminoethanethiol

AFM: atomic force microscopy

AONP: aluminium oxide nano-particles

APTMS: 3-aminopropyltrimethoxysilane

ATP: 4-aminothiolphenol

Cal-4: 4-tert-butylcalix[6]arene

Cal-6: 4-tert-butylcalix[6]arene

CCD: cooled charge-coupled device

CV: cyclic voltammetry or coefficients of variation

Δm: mass change

DA: dealloyed

DMCPS: decamethylcyclopentasiloxane

f: resonance frequency

FITC: fluorescein isothiocyanate

GPTMS: 3-glycidyloxypropyltrimethoxysilane

hIgG: human immunoglobulin G

HMDS: hexamethyldisiloxane

ICA: independent component analysis

k: spring constant

LOD: limit of detection

MBA: o-mercaptobenzoicacid

MC: microcantilever

MCA: microcantilever array

MEMS: micro-electromechanical system

MP: 3-mercaptopropanol

MPA: 3-mercaptopropanoic acid

MUA: 11-mercaptoundecanoic acid

ODTMS: octadecyltrimethoxysilane

OMTS: octamethyltrisiloxane

PDPP: poly(diphenoxyphosphazene)

PEI: poly(ethyleneimine)

PMDS: pentamethyldisiloxane

PSD: position sensitive detector

PVD: physical vapor deposition

RP: responsive phase

σ: surface stress

SAM: self-assembled monolayer

SEM: scanning electron microscopy

SERS: surface enhanced Raman spectroscopy

SG: smooth gold

SPM: scanning probe microscopy

Squ: squalane

SVM: support vector machines

TBATS: tetrabutylammonium p-toluenesulfonate

TMOS: tetramethoxysilane

VCSEL: vertical cavity surface emitting laser

VOC: volatile organic compound

CHAPTER 1: INTRODUCTION TO MICROCANTILEVER SENSORS

1.1 Micro-electromechanical Systems and Cantilevers

According to accomplished definitions, a chemical or biological sensor consists of a physical transducer and a chemically selective layer so that measurable output signals can be produced in response to biological or chemical stimuli. During the last three decades, as an "ideal" transducer, micro-electromechanical systems (MEMS) have facilitated development of sensors that involve transduction of mechanical energy and relied heavily on mechanical phenomena [1-6]. Functionality of MEMS sensors is based on mechanical movements and deformations of their micro-machined components, such as single-clamped suspended beams or suspended diaphragms

Cantilever structures similar to atomic force microscopy (AFM) probes are among the simplest MEMS. Since the advent of scanning probe microscopy (SPM), a variety of sophisticated probes were developed with extensive efforts applied on converging areas of science and technology, not only for SPM but also for cantilever-based chemical and biological sensors. [7-11].

MEMS sensors can utilize electronic, optical or other means to measure chemical and biological stimuli [12]. In particular, microfabricated cantilevers together with read-out means that are capable of measuring 10^{-12} to 10^{-6} m displacements could operate as detectors of surface stresses [13-15], extremely small mechanical forces [16], charges [17], heat fluxes [18], and IR photons [19]. As this approach reaches the nanoscale in dimension, the mechanical behavior of the cantilever starts resembling vibrational modes of molecules and atoms. Specifically, it is possible to attain

extremely high fundamental frequencies approaching those of vibrational molecular modes. Nanomechanical resonators with a mass of 2.34×10^{-18} g and a resonance frequency of 115 MHz were fabricated and displacement of 2×10^{-15} $mHz^{-1/2}$ was measured [20]. Mass sensitivity as low as a few femto-grams was reported recently using nanoscale resonators [21].

The research presented herein mainly focused on MEMS sensors with transducers in a form of microscale cantilevers.

1.2 Evolution of Microcantilever (MC) Transducer

As early as the 1920s, studies of mechanical phenomena associated with changes in a system's chemical environment were carried out, with preliminary development of the elastic theory by Timoshenko [22] and experimental studies of thin films by Stoney [23], which appeared to be significant in developing fundamental analytical models that would subsequently find wide applications in MEMS. A description of a chemical detector based on a cantilever mechanical transducer appeared in 1943 [24] with a further refinement described in 1969 [25]. Mechanical stresses and deformation produced in response to a changing chemical environment have also drawn attention as a principle of powering miniature mechanical devices [26, 27].

However, implication of these devices was limited until MEMS technology opened the opportunity to fabricate miniaturized mechanical components routinely and more precisely [28]. Although macroscopic cantilever transducers were proven to be sensitive early in the 20^{th} century [29], their extremely high susceptibility to external vibrations restricted applications. Moreover, the optical means used for measuring

mechanical responses could not provide the accuracy and sensitivity required for chemical and biological sensors [30]. In the 1960s, with the idea of "resonance gate transistor" firstly introduced [31], mechanical oscillation of a resonating microscale cantilever could be converted into an oscillatory electronic signal and amplified by the field effect transistor. This represented a successful implementation of a microfabricated cantilever transducer integrated with an electronic readout.

Nevertheless, the scope of this implementation was not related to chemical sensors until the advent of AFM in the mid 1980s [32], which is an important milestone in nanoscience and technology. AFM relied on MCs as transducers for its numerous imaging modes including topographical, electric potential, magnetic, and force imaging [33, 34]. As a natural succession to their application as force transducers in AFM, MCs were selected as a new platform for transduction in sensing technology more than a decade ago [35]. The mechanism that translates various environment components into the measured parameters such as cantilever deflection, resonance frequencies changes, and damping characteristics are generally quite different from the mechanisms that are operative in AFM. Ever since, MC sensing technology has emerged to find important applications in chemical, biological, and physical sensing.

1.3 Operation Modes of MC

In the absence of external gravitational, magnetic, and electrostatic forces, MC deformation is unambiguously related to a gradient of mechanical stress generated in the device. Based on measured parameters, cantilever deflection or resonance frequency, the operation mode of MC can be defined as either static or dynamic,

respectively. The static mode of deflection occurs when an adsorbed species causes differential surface stresses on the opposite surfaces of the MC, while the dynamic mode of detection occurs when the frequency of vibration of the beam changes as species are adsorbed onto the MC and mass changes.

A MC can be modeled as a cantilever beam (thickness, *t*; width, *w*; and length, *l*), which is built in and fixed at one of its ends (see Figure 1). Note that, *z* denotes the deflection in the thickness direction along the beam length.

1.3.1 Heat Mode

Bimaterial MCs comprised of two layers can exhibit bending with change in temperature due to thermal expansion differences. This very well-known phenomenon is frequently referred to as the "bimetallic effect" [25, 36]. In reference to the MC-based sensors, this mode of operation is frequently referred to as 'heat mode' [35]. Due to the differential thermal expansion, silicon nitride cantilevers, for example, with a thin gold film on one side undergo measurable bending in response to extremely small temperature changes due to dissimilar thermal expansion of the silicon nitride cantilever and the gold coating [37]. Heat change can be either caused by external influences, such as change in environmental temperature (thermal detection) or occuring directly on the surface by virtue of exothermic or endothermic chemical process (e.g. adsorption of analyte on the MC surfaces).

1.3.2 Static Deflection Mode

Apart from the heat produced by the adsorption of the analyte species onto the MC transducer, molecular adsorption processes and interfacial chemical reactions may

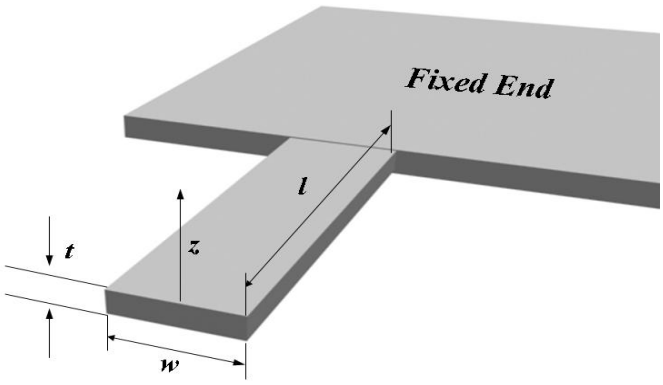

Figure 1. MC geometry and nomenclature.

also affect mechanical stresses of MC more directly and independently of the thermal effects. It has been known since the 1960s that molecular and atomic adsorbates on atomically pure faces of single crystals tend to induce significant surface stress changes. Long before the first microfabricated cantilevers were created, changes in surface stresses in these systems had been studied by measuring minute deformations of relatively thin plates. Using this method, often referred to as the beam-bending technique [38, 39], Kosch *et al.* [40] studied surface stress changes induced by adsorption of atoms on atomically pure surfaces in vacuum. Using the Shuttleworth equation [41], the surface stress σ and surface free energy γ can be interrelated:

$$\sigma = \gamma + (\frac{\partial \gamma}{\partial \in}) \qquad (1)$$

where σ is the surface stress. The surface strain $d\in$ is defined as the relative change in surface area $\partial\in = \partial A/A$. In many cases, the contribution from the surface strain term can be neglected and the free energy change approximately equals the change in surface stress.

The asymmetry of a functionalized top surface and a passive bottom surface is especially important for the static deflection mode. The MC flexural behavior is controlled by the spring constant k of the cantilever, which is defined by material properties and MC geometrical dimensions. For the rectangular MCs used in this dissertation research work, the spring constant k is calculated as follows:

$$k = \frac{E w t^3}{4 l^3} \qquad (2)$$

where E is Young's modulus. Actual spring constants can be calculated and measured for various complicated shapes and compositions by using a range of theoretical and

experimental approaches [42].

Assuming that uniform surface stress (Δσ) over the whole area of the cantilever is the cause for bending, the shape of the bent MC can be approximated as part of a circle with radius R given by Stoney's equation [23]

$$\frac{1}{R} = \frac{6(1-\nu)}{Et^2}\Delta\sigma \qquad (3)$$

where ν is the Poisson's ratio. Knowledge of the radius of curvature *R* allows the tip displacement of a MC with length *l* tip to be determined by

$$\Delta z = \frac{1}{2}\frac{l^2}{R} = \frac{3l^2(1-\nu)}{Et^2}\Delta\sigma \qquad (4)$$

For a given deflection, the surface stress change (schematically represented in Figure 2) can be derived by using Equation 3 and 4, which is, however, valid only for a surface layer much thinner than the beam itself [23]. The predictions for the cantilever bending can be based on the expected surface stress change. There have been several attempts to modify Stoney's equation for thicker layers, the accuracy of which has been reviewed in a recent article [43].

Static deflection operation is possible in various environments such as vacuum, ambient, and fluidic. In a gaseous environment, molecules adsorb on the functionalized sensing surface and form a molecular layer, provided there is affinity for the molecules to adhere to the surface. In general, however, static-mode operation in gases and liquids usually requires rather specific sensing layers to interact with special analyte, based on molecular recognition such as, DNA hybridization or antigen-antibody recognition (liquid case).

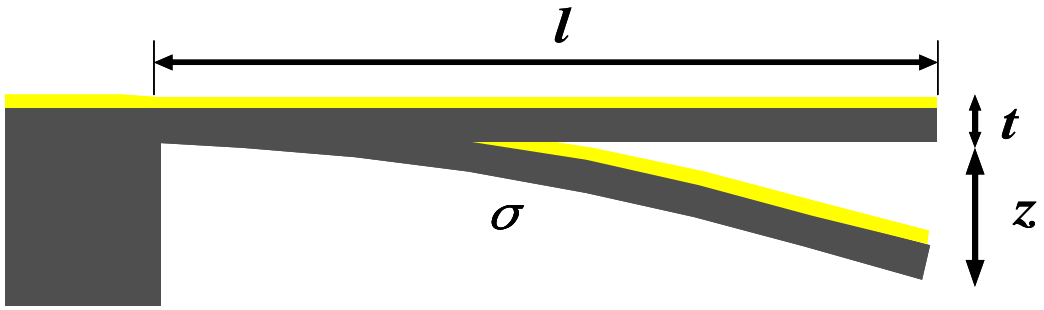

Figure 2. Schematic representation of MC deflecting in static mode under surface stress.

1.3.3 Dynamic Resonance Frequency Shift Mode

By oscillating a MC at its eigenfrequency (f_0, the resonance frequency of an oscillating MC is constant if its elastic properties remain unchanged during the molecule adsorption/desorption process and damping effects are negligible), information on adsorption or desorption of mass can be obtained under the prerequisite that the molecules on the surface are in a dynamic equilibrium with molecules from the environment.

The corresponding mass changes can be determined by tracking the change in eigenfrequency (Δf) of the MC during mass adsorption or desorption. In this dynamic mode, MC is used as a microbalance, with added mass on the surface causing the resonance frequency to shift to a lower value. The mass change (Δm) on a rectangular cantilever during molecular adsorption is related to the resonance frequency shift according to [44]

$$\Delta m = \frac{k}{4\pi^2 n}\left(\frac{1}{f_0^2} - \frac{1}{f_1^2}\right) \qquad (5)$$

where n is a geometric parameter and f_1 the eigenfrequency after the mass change.

Mass-change determination can be combined with variable but controlled temperature to facilitate "micromechanical thermogravimetry" [1]. In the mass-balance mode, the sample under investigation is mounted at the apex of the cantilevers, however, its mass should not exceed several hundred nanograms.

Dynamic mode works efficiently in the gas phase where the quality factor ($Q=f_0/\Delta f$) remains virtually unchanged as compared to vacuum (the resonance frequency shifts by a few percents). However, in liquid environment, this approach

suffers from substantial damping of the cantilever oscillation due to high viscosity of the surrounding medium increasing drag forces significantly. As a result, the resonance frequency shift is difficult to track with high resolution resulting in overall sensitivity decreases. Moreover, in the case of damping or changes of the elastic properties of the cantilever during the experiment, the measured resonance frequency will not be exactly the same as the eigenfrequency, and the mass derived from the frequency shift will be inaccurate. Dynamic operation in large damping environment is described in detail elsewhere [45].

1.3.4 Other Modes and Temperature Effects

Until now, only pure bending of a MC beam (vertical motion) has been discussed. Lateral and torsional motions can also be modeled [46] in similar manners to those presented above but will not be described herein.

In addition, thermomechanical noise [31] (vibration due to thermal agitation), the consequence of a MC being in thermal equilibrium with its environment, also needs to be mentioned. Energy dissipation in a MC usually causes the stored mechanical energy to be converted into heat. The interaction of the MC with the many microscopic degrees of freedom in its environment will subject the MC to constant random excitation. It is critical that calibration and operation of MC be performed at the same temperature and that the temperature is controlled within very tight tolerances. In the absence of temperature control, differential measurements utilizing pairs of coated and uncoated MCs must be performed.

1.4 Detection Schemes

Operation of any cantilever sensor relies on real-time measurements of cantilever deflections with at least nanometer accuracy. Therefore, an important part of any cantilever sensor is a readout system capable of monitoring changes in one of the parameters directly related to the cantilever deflection, including cantilever tip position, spatial orientation, radius of curvature, and intrinsic stress. The detection schemes employed for MC sensors can be classified broadly as optical (optical lever and interferometry) and electrical schemes (piezoresisitve, piezoelectric, capacitance, electron tunneling). All of the readout schemes are compatible with array formats.

1.4.1 Optical Lever

The optical lever technique in which light is reflected from the back of the MC onto a position sensitive photo-detector is similar to the readout scheme widely used in commercial AFM systems [47]. The deflection of the cantilever is thus translated with excellent readout efficiency into photodiode output voltage which, with proper calibration, can be converted into actual z-deflection (Figure 3). This technique, which offers a very low limit of detection (LOD) that can be better than 1 Å, was successfully adapted for the detection of static and dynamic signals in MC based sensors. Moreover, this method has already been extended to cantilever arrays using multiple lasers [48]. An intrinsic limitation of this technique is that the laser diode, positioning system, and detector must be external to the light-scattering air or fluid stream passing by the cantilever. Also, this technique is ineffective when the sample passing over the cantilever absorbs or scatters light, e.g., smoky air streams [49], and fluids with

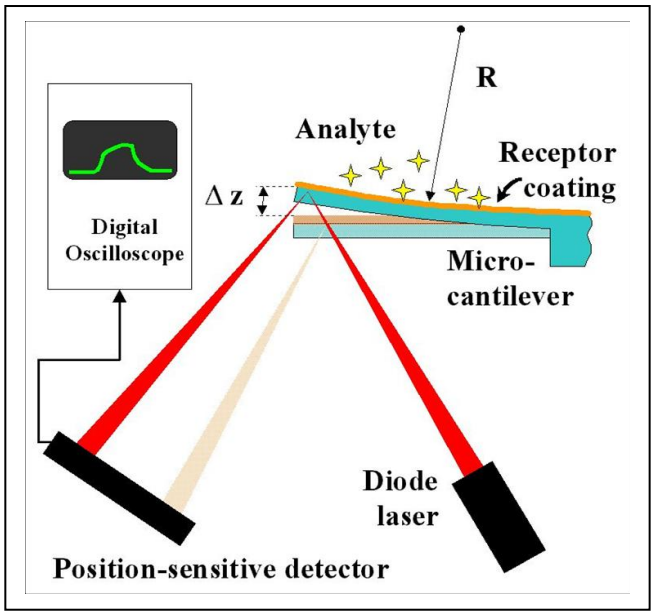

Figure 3. Optical detection scheme of MC sensor.

suspended particles [50].

In this dissertation work, the optical detection method was used to monitor the MC static deflections.

1.4.2 Interferometer

Interferometric detection of cantilever deflection is based on constructive and destructive interferences that occur when a collimated beam of light reflects off two surfaces displaced from one another [51]. In the majority of the applications of this technique, cantilevers containing a deformable diffraction grating consisting of a reference and movable set of interdigitated fingers were used. Compared to the optical lever technique, interferometer usually offers higher bandwidth measurement and has been introduced as a MEMS-based technique which shows a great promise for the readout approach for large 2-dimensional MCAs [16, 52]. This method can also be used for high-temperature vibration sensors but it has a very limited dynamic range.

1.4.3 Piezoresistive

The electrical conductivity of a piezoresistive material changes when stress is applied to it. In this method, a piezoresistive element is integrated or deposited onto the cantilever [53] during fabrication and the change in resistance is measured when the cantilever is bending. This bending also causes the induction of transient charges which are translated into a change in voltage. This method obviates the need for complex alignment procedures which is a serious problem in optical based detection methods. It also offers freedom from the bulky optical instrumentation and inconsistencies of laser alignment, and facilitates the measurement of a larger

deflection range than optical method. However, low resolution, continuous thermal drift in MC response, and additional expensive and cumbersome steps in the fabrication process make this method less common than the optical methods.

1.4.4 Capacitive

Another approach of cantilever deflection, capacitance method, is based on the principle that a change in the distance between the capacitor plates effectively changes the overall capacitance of the device. The deflection of the MC is measured by the changes in the capacitance between a conductor electrode and the MC substrate [54, 55]. Despite its simplicity, this method suffers from undesired interference effects and the change in the dielectric medium between the capacitor plates which also changes the capacitance along with gradual discharge.

1.5 Fabrication of MCs

Traditionally, MC sensors have been fabricated by a photolithographic process and bulk micromachining or surface micromachining of single crystal silicon, polycrystalline silicon, silicon nitride, or silicon dioxide, producing structures with a wide range of lengths from 100 to 500 μm and a thickness of 0.5 to 5 μm. These dimensions and materials result in spring constants ranging from 0.001 to 0.1 N m^{-1} [56]. The micromachining process for silicon-based cantilevers comprises four main techniques that, when used in combination, yield multiple cantilever chips with the desired shape and mechanical properties. These techniques are film deposition, photolithography, etching, and doping [57]. The actual fabrication sequence and the shape of the cantilever usually depend upon the detection scheme. In this dissertation

research work, commercially available MCs made of silicon were used. There have been several recent reports [58, 59] where other non-traditional materials such as metals, polymers, and nanocomposites have been employed to obtain cantilever structures, but will not be discussed in this work.

1.6 Modification of MCs

After being fabricated, to achieve selectivity in response, one side of the MC must be modified to promote binding of desired analytes to the surface and inhibit interfering substances from doing so. The other side should be kept passive to obtain large amplitude of MC deflection.

1.6.1 Surface Modification Methods and Response Mechanisms

There are three methods developed for understanding how chemical or biological stimuli impart surface stress changes to a modified MC (Figure 4). The first method is to immobilize layers (monolayer or multi-layers) onto the MC surfaces [60, 61]. The stimuli may adsorb through non-covalent interactions (e.g., van der Waals forces, dipole-dipole) or chemical bonding onto the surface layer. The second method is to coat MC surfaces with porous and thick analyte-permeable films [62]. As the analytes penetrate the films, forces including dispersion, electrostatic, steric, osmotic, and solvation can be altered by the invading analyte molecules. The alteration of these forces in the coated films can cause stress changes which are imparted to the MCs causing deformations. The in-plane component of the film stress can be multiplied by the coating thickness to give an apparent surface stress change, which can be applied to Stoney's equation. The third method is to nanostructure the MC surfaces [63]. In

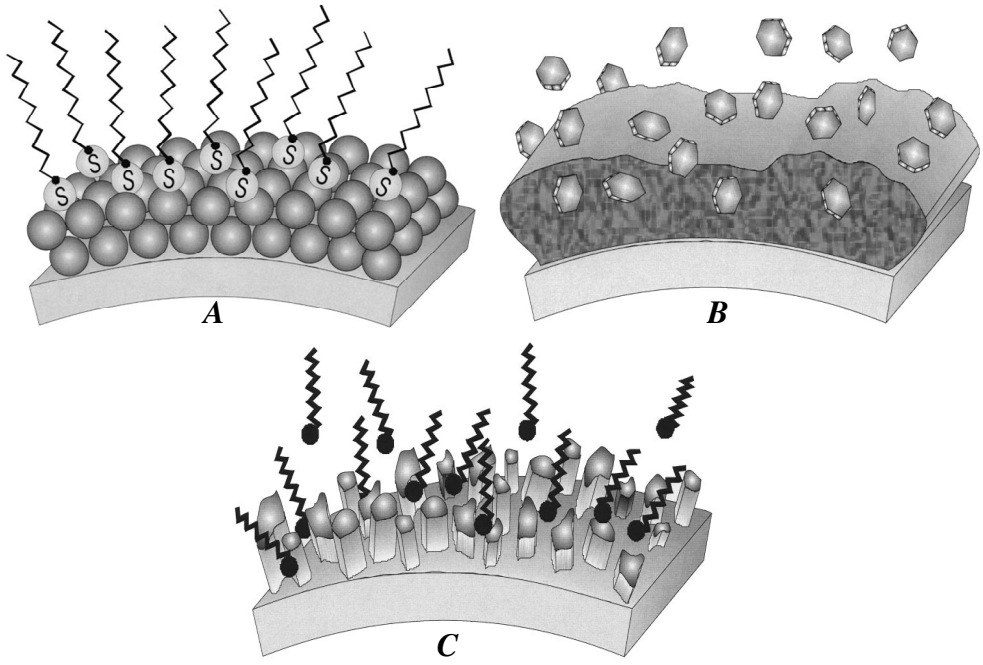

Figure 4. Schematic depiction of (A) immobilization of thiol monolayer on a gold coated MC surface, (B) analyte-induced deformation of MC coated with an analyte-permeable thick film, (C) analyte-induced deformation of MC coated with a nanostructued modifying phase.

nanostructured phases, analyte-induced stresses combine bulk, surface, and inter-surface mechanisms resulting in large stress changes and large amounts of MC deformations. Estimates of the mechanical energy produced by a nanostructured MC can be calculated. The product of the energy associated with the phase-analyte interactions and the number of interactions can be used to estimate the mechanical energy.

1.6.2 Types of Phases

Inorganic and organic materials are used to modify MC surfaces with the three methods discussed above.

Numerous reports used inorganic materials such as metals or metal oxides as active absorbing layers for preferential sorption of the analytes [58, 64, 65]. These materials are deposited onto MC surfaces by either sputter coating or thermal evaporation [66]. In order to obtain enhanced surface area and achieve better partition of target analytes for enhanced sensitivity, MCs can be coated with films having nanocavities [67] or granular nanostructure [68, 69].

However, those bimaterial cantilevers are limited in their applications due to their limited chemical functionality and affinity to common target molecules. For improvement, organic and biological reagents have been applied as responsive coatings to detect various physical, chemical and biological stimuli [70-75]. These species include monolayer of ligands and biomolecules (DNA, specific antibodies, polypeptides, nucleotides), lipid layers, polymers, polymer/other nanocomposites, hydro-gels, and sol-gel multi-layers. Constructions of these organic phases can be

accomplished through various methods such as drop casting [76, 77], spin coating [78], inkjet printing [79], spray coating [80], capillary painting [81], plasma polymerization [82], *in situ* polymerization [83, 84], *grafting to* via monolayer functionalization [85], and matrix assisted pulsed laser evaporation [86]. In particular, responsive organic coatings are important to optimize several key attributes, specifically high sensitivity, good selectivity, fast response time, wide dynamic range, and long shelf life critical for their ultimate performance.

In summary, this chapter briefly discusses MC sensors, including historical evolution, operation modes, detection schemes, fabrication and modification of MCs. For what has been accomplished in this dissertation research work, only static mode and optical detection method were applied. No research on MC fabrication was carried out and the research goals of our group primarily focus on modifying the commercially available MCs to obtain higher selectivity and sensitivity. This dissertation work involves utilizing two different types of nanostructured MCs for chemical and biological sensing. Those modified MCs with high surface area were functionalized by immobilizing self-assembled monolayers (SAMs) of binding sites or coating organic responsive phases (RPs) onto the nanostructured surfaces to recognize specific target analytes. Moreover, in order to get enhanced and distributed selectivity, the MCs in the same sensor chip were differentially functionalized to make a true MC multi-sensor array which can recognize more than one target analyte simultaneously.

The next chapter will give a brief discussion on MC sensing arrays, mainly focusing on array preparation, and data analysis algorithm related to this dissertation

research work. A short summary of recent applications of MC sensors and MC multi-sensor arrays will also be included.

CHAPTER 2: MICROCANTILEVER SENSING ARRAY

During the last ten years, there has been a trend to use chemical and biological multi-sensor arrays such as metal oxides sensing films [87], electrochemical sensors [88], conducting polymer sensing materials [89], quartz crystal microbalance devices [90], field effect transistor devices [91], and surface acoustic wave devices [92], to recognize individual components in mixtures. Further advantage of the multi-sensor array concept has been achieved by using MC transducers because MC features superior mass sensitivity, smaller size, lower cost, and excellent compatibility with large multi-sensor array platforms [93, 94]. MCAs with distributed partial specificity and selectivity towards various classes of compounds, used in conjunction with pattern recognition techniques, allows for the identification and quantification of individual chemical and biological components in mixture samples. MCA essentially recognizes the chemical fingerprint, which is the global chemical and biological information of the sample or classes of samples to be recognized.

2.1 Preparation of MCAs

Coating individual cantilevers within arrays can be the most essential challenge that needs to be considered as pre-requisite for any studies on MC sensing arrays. Up to now, there are four approaches that have been proven useful for functionalizing multiple cantilevers in the same sensor chip: inkjet printing, contact printing, capillary arrays, and selective deposition. The last two methods were used in this dissertation work.

2.1.1 Micro-inkjet Printing

Micro-inkjet printing affords efficient and controlled functionalization of only one side of the cantilever, and the whole functionalization process is fast and modestly destructive [79]. This technique can be used for both immobilizing SAM and coating porous or nanostructured phases onto MC surfaces. Generally, this technique involves pipetting small drops (μL or nL) of solutions or uniform mixtures onto one side of MCs, and the solutions or mixtures were prepared with the materials for coating and suitable solvents (Figure 5). With evaporation of the solvents, SAMs, films or nanostructured phases will functionalize the MC surfaces through either physical adhesion or chemical reactions. Cross-linking process takes place most commonly on the surfaces, through which condensation and polymerization (methods also referred to drop-casting) via covalent bonds was achieved for immobilization and growth of the phases.

However, meticulous alignment is required for ink jet printing. Reproducibility for modification was sometimes not satisfactory (Figure 5) due to no control over microstructure or thickness of the coated layers [79]. High expense of the systems is another issue. Commercial micro-inkjet printing systems are available from several manufacturers (e.g., Cantisens and Microdrop Technologies) currently.

2.1.2 Contact-printing

Differential modification of MCs can also be applied by contact-printing methods such as using dip-pen lithography [95-97]. It is a scanning probe lithography technique where an AFM tip is used to transfer molecules to a surface via a solvent meniscus. It

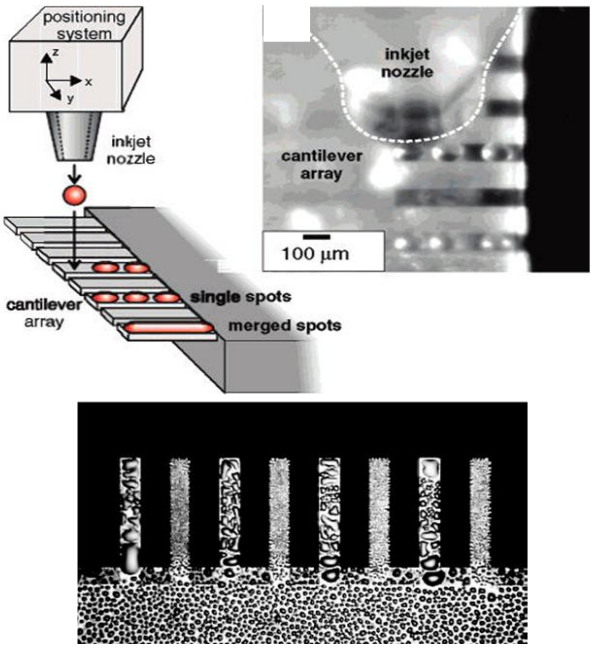

Figure 5. Ink-jet printing of responsive layers on an MCA, optical micrograph of the process, and condensation of water on cantilever array coated with hydrophilic and hydrophobic layers. Reproduced from Bietsch et al., *Nanotechnology* **2004**, *15*, 873.

enables direct deposition of nanoscale materials from the tips onto MC surfaces and different MCs within the same array can be modified through contacting with different printing tips. However, similar to ink-jet printing technique, meticulous alignment and high system expense are the primary drawbacks of this technique. Commercial dip-pen lithography systems are available from BioForce, NanoInk, and Nanonics Imaging.

2.1.3 Capillary Arrays

This method involves inserting the desired cantilever into a capillary filled with reagent using a micromanipulator. The capillary must have an internal diameter larger than the width of the MC beam, and the wall of the capillary must be thin enough to fit between the MC beams in the array. The capillary is held in place for an allotted amount of time required for functionalization and then retracted.

When several different MCs in the same sensor chip require functionalization to make a multi-sensor array, all cantilevers within the array can be simultaneously inserted into an array of capillaries using an appropriately designed micromanipulator (Figure 6) [98,99] which can be home-made. It needs to be mentioned that both sides of the cantilever are wetted using this approach. Thus, if only one side of the cantilever is to be modified, then the reaction chemistry of the fluid within the capillary must be designed to react only with the desired region. The most attractive advantage of this method is low cost.

2.1.4 Selective Deposition

This method is used in our research work for preparing a MCA differentially

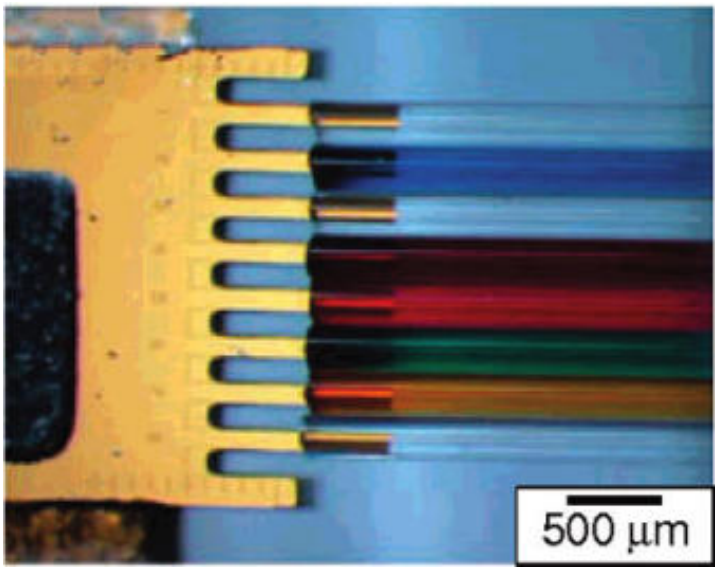

Figure 6. Immersion of a cantilever array into an array of glass microcapillaries filled with food coloring for demonstration purposes. Reproduced from Bietsch et al. *Nanotechnology* **2004**, *15*, 873.

coated with various organic RPs. Thermal evaporation was used to coat the phases onto the MC surfaces and a mask with one or more slits slightly wider than a MC beam was used to preferentially expose MCs to the vapor at a time. The mask can also be used when MCs are modified with some other approaches such as spin coating. Tight enough touching between the unexposed MCs and the mask can avoid cross contamination, and this method can be tedious and time-consuming if many different phases are coated onto the same MCA. RPs' volatility may be an issue to the phase stability and MC response reproducibility, although related studies have not been carried out yet.

2.1.5 Integrated Microfluidic-MCA Platform

As an extension of our most recent and ongoing efforts in the area of MCAs, we have begun creating advanced MCAs integrated into μ-fluidic chip platforms that allow convenient differential functionalization of individual MC element using flow of reagents that originates from the multiplexed (non-common) side of the fluidic device. We believe suitably engineered and integrated μ-fluidic-MCA systems will greatly enhance applicability of the MC sensors to studies that will advance biosening research. Figure 7 illustrates the basic architecture of the integrated MCA-μ-fluidic chip. Fabrication of the targeted integrated MCA-μ-fluidic systems will rely on a combination of photolithographic patterning, dry and wet etching, and thin film deposition.

Using flow from the common ends, differential systems can be exposed to the same sample component. Conversely, independent flow from the functionalization

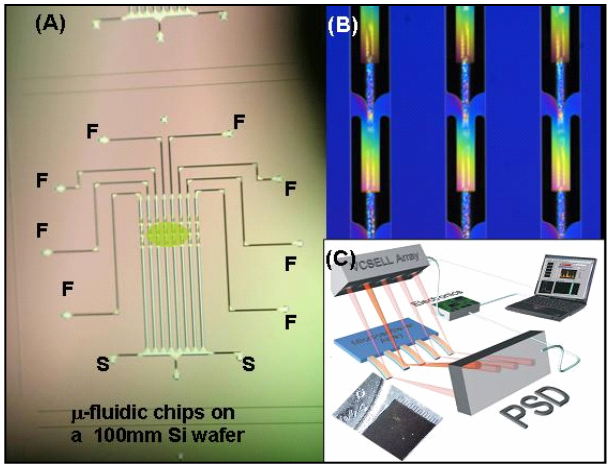

Figure 7. μ-fluidic platform consisting of several parallel channels (~200 μm wide & 20 μm deep) housing silicon nitride free standing MCs (see B). Individual reservoirs mate to the channels and permit each set of MCs to be functionalized (via Fs) independently. Samples can be delivered via the S reservoirs to create response patterns. The patterns are generated by tip deflections causing VCSEL beam deflections onto a single position sensitive detector (see C).

ends (F) can be used to differentially modify the MC in different channels. Among the additional advantages of this approach are high throughput, extremely low volume, the possibility of convenient ambient control (temperature, pressure), and systems that can be regenerated for reuse. These future advanced integrated systems are not the focus of this dissertation work.

2.2 Detection and Data Analysis Algorithm

It has been mentioned that the four primary detection schemes are all compatible with array format, and that the optical method is most widely used in MC sensing array systems. A general schematic of a MC multi-sensor array are depicted in Figure 8. Besides a MCA differentially modified on the active sides, it also includes an array of photon source, such as parallel lasers, and an optical position sensitive detector (PSD), such as a cooled charge-coupled device (CCD) or a quadrant photodiode, which responds to spatial changes of the laser beams. Because the bending extend of all MCs is diverse due to specific interactions between each distinctively modified MC and target analytes, the readout of the MCA is a complex multi-dimensional signal that must be analyzed using advanced mathematics. At this stage, realization of the full potential of MC sensing arrays depends largely on the availability of a suitable data analysis algorithm.

The construction of MC multi-sensor array makes the readout signal specifically amenable to independent component analysis (ICA). The concepts surrounding ICA were first introduced in 1991 by Jutten et al. [100] and later formalized in 1994 by Comon [101]. Over the course of the last decade, ICA has proven to be a powerful

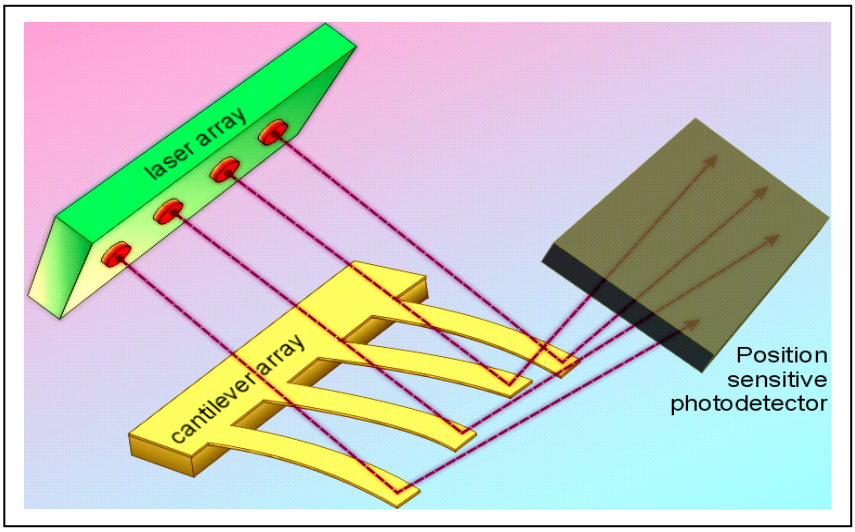

Figure 8. Optical readout of a MCA using an array of lasers.

technique in many different applications. It can provide a (linear) sparse coding representation of natural image data [102], and has also been adopted in bio-medical imaging [103]. It is a natural extension to adapt the ICA method to extract features and information for the present analysis of MC sensing arrays.

It will be briefly discussed how ICA can be used as a data pre-processing method for neural network classification of MC multi-sensor data. Appropriate coupling of these mathematical methods can accurately capture information contained within the array of MC sensors to identify chemical mixtures and concentrations and decode mixtures of analytes. As a result, the usefulness of MC multi-sensors can be greatly increased for complex applications.

Suppose that $x(t)$ represents an N-dimensional measured time series vector of sensor signals. Assume that linear mixing of independent sources produces this measured data, or

$$x(t) = As(t) \qquad (6)$$

$s(t)$ is the M-dimensional time series vector of independent sources and A is the $N \times M$ mixing matrix. Further assume that $M \leq N$ and A has full rank. ICA is a de-mixing procedure that, given only the measured data $x(t)$, recovers W, the mixing matrix, such that

$$W = SPA \qquad (7)$$

Here, S and P are scaling and permutation matrices, respectively. Amazingly, under these assumptions, both the mixing matrix and corresponding sources can be recovered based only on the knowledge of the measured data, to an arbitrary scaling and

permutation. For systems where the measured data is the linear mixing of independent sources, ICA is a tool that can transform measurements into source information.

For MC multi-sensor arrays, the feature extraction capability of ICA is used to pre-process readout data from MCAs in order to concisely portray this information to the neural network for classification. Specifically, the multi-dimensional signal produced from the bending of the MCAs is used as the measured data in the ICA method. Columns of the estimated mixing matrix are used as features, providing a vectorized input for neural network classification.

However, direct input of the entire signal, without pre-processing, will overwhelm the network resulting in poor classification accuracy, and in this feature extraction procedure ICA can only determine the mixing matrix to an arbitrary scaling and permutation. It is necessary to impose a systematic procedure that induces consistent scaling and permutation, which will not be discussed in detail in this work.

The nature of the MCA system lends itself to analysis from ICA which has two significant properties. First, the dominant features depend strongly on the MC-analyte interactions. Second, the dominant sources are similar across both chemical species and concentration. The explanations of these properties can be traced to the physics of the cantilevers. Since differentially modified MCs will respond differently to a given analyte, these attributes will translate to the feature space. The estimation of similar sources stems from the fact that each cantilever to a certain degree undergoes similar types of characteristic bending, a direct result of the fundamental interfacial

interactions between the transducer and the analyte. In other words, each source corresponds to distinctive bending dynamics that, in turn, can be ascribed to specific physical and chemical processes involved in the MC-analyte interactions.

The vector structure of the extracted features can be exploited for efficient recovery of the identities and concentrations of the constituents of a sample mixture from its MC fingerprint. Each column of the mixing matrix represents an independent feature of the data, and a subset of the columns is sufficient for input to an artificial neural network.

A premier method of data modeling and classification over the past two decades involves the use of neural networks. Since these methods have been extensively reviewed in the literature, a brief summary is all that is needed herein. Back propagation networks were created with the MATLAB® Neural Network Toolbox. The typical architecture contained a single hidden layer and employed the hyperbolic tangent sigmoid transfer function for the input and hidden layers and the linear transfer function for the output layer. Training was accomplished through the Levenberg–Marquardt algorithm, a variant of Newton's method. Training was halted at a specified tolerance value.

2.3 Applications

Several reviews have been published over the past decade on applications of MC as a sensor platform for chemical and biological sensing [104-107]. Currently, MCAs enable to control experiments to be performed simultaneously with analysis. They can also provide more reliable control of empirical factors such as thermal drift,

changes in viscosity, and solution flow dynamics. What's more, MCAs can detect more than one analyte simultaneously with distinct recognition patterns produced from complex mixtures [108]. Therefore, MC multi-sensor arrays have already become a preferred format.

During the past several years, applications of MC multi-sensor arrays include analysis of volatile organics [72], chemical warfare agents [109], volatile organic compounds (VOCs) [110] and toxic inorganic ions [111] for chemical sensing, while efforts are put into the studies of cells [112, 113], virus [114], antigen-antibody interactions [105], and DNA Hybridization [115] for biological sensing. More details of recent MCA applications can be found elsewhere [116, 117] and will not be discussed further in this work.

In the next two chapters, we will use two different MCAs to analyze some gas and liquid phase samples. The MC surfaces of the arrays were modified into a nanostructured surface with the approach developed by the previous group members. Consequently, the two arrays were differentially modified with capillary array and selective vapor deposition, respectively. High sensitivity and enhanced selectivity are obtained from both arrays.

CHAPTER 3: DIFFERENTIALLY FUNCTIONALIZED MCA FOR METAL ION SENSING

Chapter 3 is an adaptation of a research article *Analytical Chemistry* **2007**, 79, 7062-7068. The article demonstrated that SAM of different thiolated ligands could be immobilized onto individual gold nanostructured MCs in the MCA for metal ion sensing, with distributed selectivity and high sensitivity obtained.

3.1 Introduction

With ever-increasing industrial sprawl, the likelihood of release of pollutants into the environment increases. Technologies for environmental monitoring must keep pace with expanding industrial demands. One class of environmental pollutants that has garnered much attention recently is that of heavy metals. Heavy metals are particularly dangerous to the entire ecosystem because not only are they toxic, but they possess the ability to bio-accumulate in organisms [118]. Bioaccumulation increases the heavy metal concentration present in an organism and therefore increases toxic effects. Heavy metal poisoning has shown to cause medical difficulties with, but not limited to, nervous, gastrointestinal, and cardiovascular systems [118]. The health threat that heavy metal contamination can pose necessitates a technology able to detect and identify metal ions present in our environment.

Currently, methods used to detect metal cations include liquid or gas phase chromatography [119-121], flow injection systems [122], electrochemistry [123, 124], atomic absorption [125], solid-phase extraction [126], fluorescent sensors [127], inhibition-based enzymatic assays [128], and immunoassay [129]. However, many of the techniques are not amenable to environmental sensing because they are expensive

and/or time consuming. Newer, more adept technologies must be produced to confront the shortcomings of older technologies.

MC sensors have emerged recently as sensing transducers that offer greater mass sensitivity than comparable sensors such as quartz crystal microbalances, flexural plate wave oscillators, and surface acoustic wave devices [130] due in large part to their very small dimensions.

Recently, MCs have shown promise in the area of metal cation detection [131]. Dutta et al. demonstrated that by functionalizing gold nanostructured MCs with thiolated ligand SAMs, the MCs would respond to different metal cations present in a sample. The ligand functionality interacted with the metal cations satisfying only a portion of the metal's coordination sphere; this allows for reversible interactions. The procedure used to nanostructure the surface prior to ligand functionalization results in good sensitivity despite the modest binding constants between the monodentated ligands and metal ions.

In this chapter, the work of Dutta et al. is expanded upon by using MCAs with multiple MCs differentially functionalizing with thiolated ligand SAMs, thereby creating for the first time a true MCA with ionic discrimination capabilities. The underlying dealloyed (DA) nanostuctured surface was created by codepositing Ag and Au and then etching the Ag from the composite layer [132]. Properties of this nanostructured DA surface such as, thickness, gold to silver deposition ratio, and etching time were more thoroughly studied and optimized. Electrochemical and in-situ derivitization experiments were performed to demonstrate the impact that DA

layer changes would have on the thiolation of the surface. Surface enhanced Raman spectroscopy (SERS) experiments were performed directly on MC surfaces to demonstrate that a capillary coating procedure could be used to successfully differentially functionalize each of the diminutive cantilevers in an array with a different thiolated ligand. Sensor performance experiments were then performed to demonstrate the sensitivity and selectivity (differentiating capabilities) of the MCA sensor. Finally, pattern recognition algorithms were applied to the selectivity studies to classify metal ions in unknown samples.

3.2 Experimental

3.2.1 Materials and Reagents

Silicon MCs with dimensions 400 μm length, 100 μm width and 1 μm thickness were commercially available (Mikro Masch Co., Sunnyvale, CA). The chromium, gold and silver metals (99.9% in purity) used in vapor deposition were obtained from Kurt J. Lesker, Gatewest, and Alfa Aesar Co., respectively. The flexible fused silica capillary was purchased from Polymicron Co. with 350 μm outer and 250 μm inner diameters. All the metal chloride analytes, salts for preparation of buffer solution, thiolated ligands (List below in Table 1), and the 4-aminothiolphenol (ATP) and o-Mercaptobenzoicacid (MBA) used in SERS experiments were obtained from either Sigma or Fisher at highest purity and used as received. HF buffer containing ammonium floride and hydrofluoric acid used for the capillary etching was purchased from Transene Company. Water used for preparation of solutions was obtained from a Barnstead E-Pure water filtration system.

Acronyms	Name of the Thiolated Ligand
AET	2-aminoethanethiol
MP	3-mercaptopropanol
Cystein	Cystein
MPA	3-mercaptopropanoic acid
MUA	11-mercaptoundecanoic acid

Table 1. Each RP used in the study is listed.

3.2.2 MC Modification

The creation of MCs having a silver, smooth gold (SG) or DA surface was achieved by using a physical vapor deposition (PVD) approach. More details about the PVD instrumentation and approach can be found elsewhere [131, 132]. DA nanostructured surfaces with a composite 50/50 Au/Ag film with different thickness of 50 nm, 75 nm, 100 nm, 150 nm and 200 nm were deposited using the PVD approach. 3-5 nm of Cr was deposited first then 15 nm of Au was deposited subsequent to the Cr. Finally, the Ag/Au composite film was created by co-deposition of Ag and Au. During the deposition, both the deposition rate and resulting coating thickness were monitored using a quartz crystal microbalance. To create nanostructured DA surfaces from the Au/Ag film, the silver was etched out of the composite film by placing the cantilevers in an aqueous solution of 0.2% w/v $HAuCl_4$ for about 2.5 min. Cantilevers were then rinsed with copious amounts of water after etching. The Ag coated cantilevers for SERS experiments were also created through the PVD approach by depositing 10 - 15 nm of Ag to create a SERS-active Ag-island film on the MC. All Ag/Au, smooth Au or Ag-coated cantilevers used in our studies were chemically modified with SAMs of *n*-alkyl compounds with a thiol group for immobilization of the ligand to the metallic MC surface on one end and monodentated ligand functionality for the complexation of sample metal ions on the opposing end.

To differentially functionalize each cantilever with different thiolated ligands (Table 2), a capillary coating apparatus was designed. The flexible capillaries were aligned and mounted horizontally in sequentially parallel channels with 500 μm spacing

Thiol Ligand Solution	Concentration (mM)
AET	25
MP	25
Cystein	10
MPA	5
MUA	1
ATP	0.01 mM
MBA	0.01 mM

Table 2. Optimized concentrations of each functionalization ligand solution.

between them using a V-groove holder machined in-house (note: the MC pitch is 250 μm so alternate MCs are aligned with the capillaries). To allow the MCs to be inserted into the capillaries, some pretreatment of the capillaries was carried out. First the polyimide coating on one end of the capillaries was burned off, and the other end was sealed with soft playdough. The burned end was then dipped in HF buffer [Caution: HF is very corrosive to skin] and etched for 100 minutes to reduce the outer diameter. The sealed end was then cut off. De-ionized water was allowed to fully fill the etched capillaries several times until the etched end appeared to be clean. Meanwhile, the nanostructured MCAs were fixed on an *x*-*y*-*z* stage, with all the levers in the direction parallel to the capillaries. Once the capillaries were inserted into the capillary ends for functionalization, the opposite end of the capillaries were inserted into the appropriate thiol solutions and filled by simple capillary action.

3.2.3 Instrumentation

During MCA functionalization, MCs and etched capillary ends were visualized with a WAT-902C camera connected to a Sony Trinitron Video Monitor, which provided a 20×magnification. All SERS spectra were collected by using a modified version of a LabRam Spectrograph from JY-Horiba [133]. The instrument used an Olympus BX-40 microscope with a 10×(0.25 NA) objective that delivers up to 8.9 mW of the 632.8 nm radiation from a He–Ne laser. The scattered light was dispersed with a 600 grooves mm-1 grating, imaged with a 1024×256 thermoelectrically CCD camera, and processed with Labspec 4.03 software. An *x*–*y*–*z* stage was used to adjust

the focusing of the microscope objective and the positioning of the laser spot under stationary and translating conditions.

MCAs were mounted in a brass flow cell in an optical system [134]. The cell had one inlet port for background/analyte delivery, one outlet port, and a glass window to facilitate the observation of cantilever deflection. A beam of laser light from an array of vertical cavity surface emitting lasers (VCSELs) (Avalon Photonics, 850 nm, 5 mW) was focused onto the tip of each MC, and the reflected beam was captured and monitored by a single PSD. A single lens was used to focus the VCSELs so that the beam from each VCSEL was focused onto a single corresponding cantilever (12 VCSELs onto 12 cantilevers). The deflection of the cantilever resulted in a corresponding motion of the reflected beam as monitored by the PSD. An in-house-created LabView program controlled a multiplexing scheme that allowed the VCSELs to be activated individually so that one MC was illuminated at a time and the motion of all MCs was monitored by the single PSD. Analyte solutions were delivered to the flow cell via a system of vessels connected to three-way valves allowing for switching between different solutions (buffer and samples) with minimal disturbances of the flow. Each measurement in the study represents a 60 second injection of a metal chloride solution. All metal chloride solutions were prepared in pH 5 acetate buffer, which was also used as a background buffer solution. Chemically modified cantilevers were allowed to equilibrate in the background solution until stable baseline was achieved before any measurements.

3.2.4 Data Acquisition and Interpretation

In the SERS experiment, the focusing laser scanned in a perpendicular direction across 4 adjacent cantilevers functionalized alternately with ATP and MBA. SERS spectra were recorded while the area interrogated moved laterally over a total 1 mm distance. For each cantilever 50 spectra were recorded (one every 2 μm translational step). For each spectra the peak height of the characteristic Raman band of ATP (1010-1050 cm^{-1}) and MBA (1055-1095 cm^{-1}) was recorded and plotted.

For MCA measurements, an in-house-created LabView program was used to control each VCSEL to be activated individually so that one cantilever was illuminated by only one VCSEL at a time. At the beginning of each cycle, the first VCSEL was activated, illuminating the corresponding cantilever 1. The motion of the reflected beam was monitored by a single PSD, and output signal from the detector was sampled by a 16-bit A/D converter at a rate of 1 kHz. 50 samples by the A/D converter were averaged to comprise one point. The sequence was then repeated for VCSEL/cantilevers from 2nd to 12th (the last). The entire cycle of measuring and recording all 12 MCs takes less than 1 s; therefore, a delay was added so that the cycles begin at 1-s intervals. VCSEL control and data acquisition I/O were performed using a National Instruments NI-6014 DAQ card in an 800-MHz Pentium III PC [135]. Although the MCA and VCSEL arrangement allows for the monitoring of all 12 cantilevers, in the selectivity studies only 5 cantilevers responses (see below), one for each phase, are represented. However, the data used by the pattern recognition

algorithm included responses from all 12 cantilevers comprising the array with each of the 5 phases represented multiple times.

Analysis of the entire response profile (responses recorded once per second for each MC during the entire 60 second analyte injection period) for the array for each metal ion was used in an attempt to classify the metal ions. Prior to classification, the information contained within the analyte-induced bending dynamics of the MCAs must be distilled into a form that can be used with existing classification methods. Since inputs for general classification method are N-dimensional vectors, it is necessary to transform the information contained within the time series response of each cantilever into a single vector. It was demonstrated in Archibald et al [134] that ICA can be used to compress the movement of an array of MC over a period of time, into a single feature, an N-dimensional vector, that was used by neural networks to accurately classify both the type and concentration of the tested analyte.

Stated simply, given only the measured motion of the MCA data, the ICA method produces the independent sources of this signal and the mixing matrix, up to arbitrary scaling and permutation of the sources. The benefit of determining this transformation is that the columns of the mixing matrix provide distinct features that can be used for accurate classification. In this metal-ion study, only the most dominant feature (the column in the mixing matrix with the greatest magnitude) is used in classification [134].

Support vector machines (SVM), a classification paradigm developed over the last decade in the field of machine learning theory [136], have proven to be an

effective tool across many scientific disciplines. In order to describe the core ideas of SVM we must consider the features described above or N-dimensional vectors, which can equally be consider as hyper-dimensional points. SVM is a binary classifier, meaning it is designed to identify only two different groups. SVM classification of two groups of features occurs by finding a surface that optimally separates these groups. Once this surface is determined, classification occurs for any new feature presented to SVM by calculating which side of the surface this point lies. The surface that optimally separates the two groups of features is termed the decision surface. A strength of SVM is that complex decision surfaces can be generated at low computational cost through the use of kernel functions, which have the effect of transposing features into spaces that increase the linear separability of the two groups of features. The geometric nature of the SVM classifier makes it possible to train adequately on reduced sets. One major drawback of SVM is that classification is binary. However, this issue is overcome in a simple and robust procedure that consists of training several SVM's simultaneously in a one-against-one scheme [137], and this is the procedure used in this chapter (see below).

3.3 Results and Discussion

3.3.1 Nanostructured Surface Characterization

In our previous studies using SAMs as a RP for metal ion detection [131], optimization of the sensor response focused on parameters concerning the SAMs. Studies involving parameters such as functionalization time, thiol concentration, thiol chain length and functionality were performed. In this present work, much attention

was paid to optimization of the underlying DA nanostructured layer. The first parameter studied concerning the DA layer was that of metal layer thickness. Experiments were carried out measuring responses of SAM functionalized DA layers to metal ions for metal layers ranging from 25 – 200 nm. Figure 9 demonstrates that as the DA thickness of the MP-coated cantilever was increased up to 150 nm, the response to 0.1 mM of Cu^{2+} also increased. However, as the DA layer thickness was further increased to 200 nm, the response decreased slightly. According to the Stoney's Equation, as the cantilever stiffness increases the response decreases (note Et^2 in denominator). The increase in DA thickness results in an increase in surface area (see below) and the $\Delta\sigma$ term in Eq. (4) that resulting from coulombic forces associated with metal-metal repulsion can be expected to increase as well [131]. However, at some point the effect of increasing stiffness (note both terms in the denominator change with DA thickness) appears to reverse (dominate) the trend due to increasing $\Delta\sigma$. Experiments involving varying the Ag/Au ratio from the normal 50/50 to 40/60 and to 60/40, along with experiments varying the dealloying etching time from 2.5 minute. to 5 and 10 minute., did not yield any improvement

Further experiments were performed to try to better understand why the increased thickness of the underlying DA layer demonstrated an enhancement in response of the MC to metal ions. Figure 10 shows the response of three different cantilevers coated with 35 nm of SG and 50 nm and 150 nm DA layers to an in-situ functionalization with a SAM of propane thiol. The 35 nm SG shows the smallest response to the formation of a monolayer of propane thiol, with the 50 and 150 nm DA responses

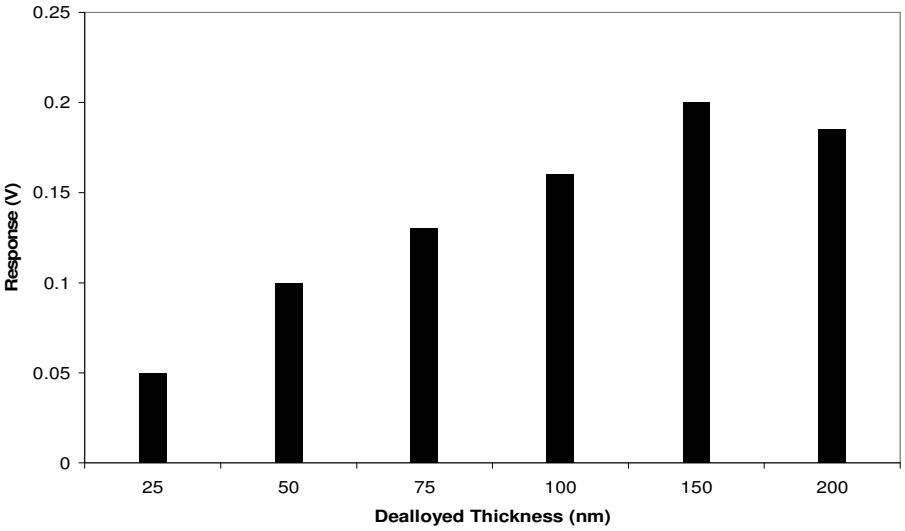

Figure 9. The effect of DA thickness was studied by monitoring the response to a 0.1 mM Cu^{2+} solution for MCs with different thicknesses of the DA layer and functionalized with MP.

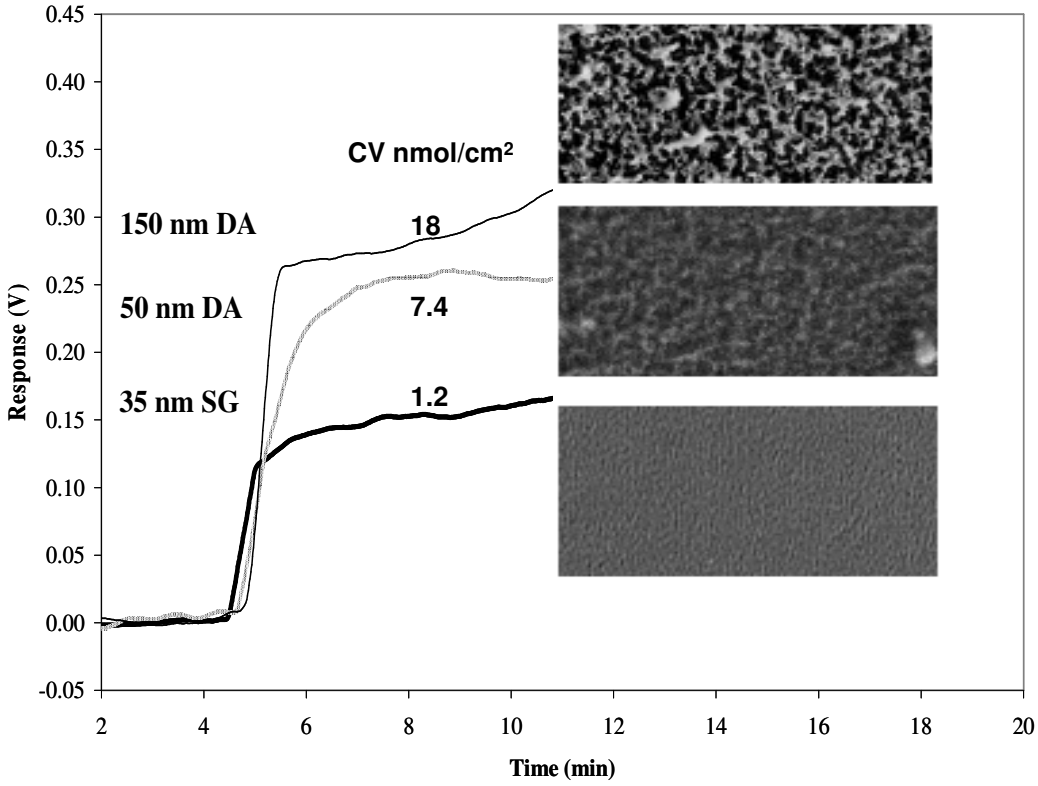

Figure 10. Surface thiolation studies were carried out by measuring the response of each cantilever (35 nm SG, 50 and 150 nm DA) to an in-situ functionalization with 1 mM propane thiol. Oxidative desorption of the propane thiol from the gold surface through cyclic voltammetry (CV) made it possible to quantify the amount of thiol on each surface. Scanning electron microscopy (SEM) images of each surface were taken at 8000×magnification.

considerably larger. A larger thickness gives a larger response to the formation of propane thiol monolayer suggesting a larger amount of thiol immobilized, but as stated above a larger DA thickness may decrease the ability of the cantilever to respond due to increased stiffness.

To quantify the amount of thiol on the each surface, CV experiments, using the strategy of Widrig et al [138], were performed with silicon wafers, which were vapor deposited and functionalized at the same time as the three cantilever types in the thickness study. The cyclic voltammetry experiments demonstrated that the 35 nm SG coated silicon wafer was coated with 1.2 nmol/cm^2 of propane thiol, while 50 and 150 nm DA surfaces were coated with 7.4 nmol/cm^2 and 18 nmol/cm^2, respectively. The larger trend in the CV values versus actual responses during functionalization with propane thiol underscores the interplay between increases in surface stress with greater surface area and the changes in stiffness. The SEM images, seen the figure, indicate the potential importance of surface morphology on determining response characteristics of the MCs. The greater the degree of roughness and surface crevices, the greater the available surface for thiol immobilized. It can be seen that the 50 nm DA has greater roughness than the SG. The thicker 150 nm DA seems to have transitioned from a roughened surface to a more porous one. Surface area may not be the only factor in determining $\Delta\sigma$ associated with functionalization and/or binding of metal as the effectiveness of translating the energies associated with those processes into potential energy stored in the bent cantilever can reasonably be expected to be morphology dependent [132].

3.3.2 Differential Array Creation

The first step in creating a differential responding MCA involves developing a method that allows differential coating of the cantilevers in an array. In our prior gas phase sensing work, differential coating was accomplished by singularly vapor depositing a RP through a slit mask onto one cantilever [134]. While this practice of sequentially depositing phases onto each cantilever does allow for creation of arrays, the process is time consuming, tedious, and the RP are not covalently anchored to the cantilever surface to enhance stability. In this work, MCAs are prepared in a liquid phase reaction process via capillary coating individual cantilevers with thiolated reagents. Figure 11 demonstrates how the capillary coating process is accomplished. The top photograph displays several cantilevers of the MCA inserted into different capillaries by way of a micrometer controlled stage. Then, in the bottom photograph, the functionalization solution fills the capillary through capillary action. The picture demonstrates that the functionalization solution was contained in the capillary and no solution leaks out on the base of the MCA chip. If solution were to leak out of the tip of the capillary, cross-contamination problems could arise and the cantilevers could be coated with more than one type of thiolated ligand. The SERS experiment in Figure 11B demonstrates that the thiolated ligand RP were in fact immobilized on the surface. In this experiment, silver coated MCs were inserted into capillaries that were subsequently filled with either ATP or MBA and allowed to react for 2 hours. After functionalization, the MCs were removed from the capillaries and SERS spectra were collected from each MC surface in a dry state by the spatial translation method

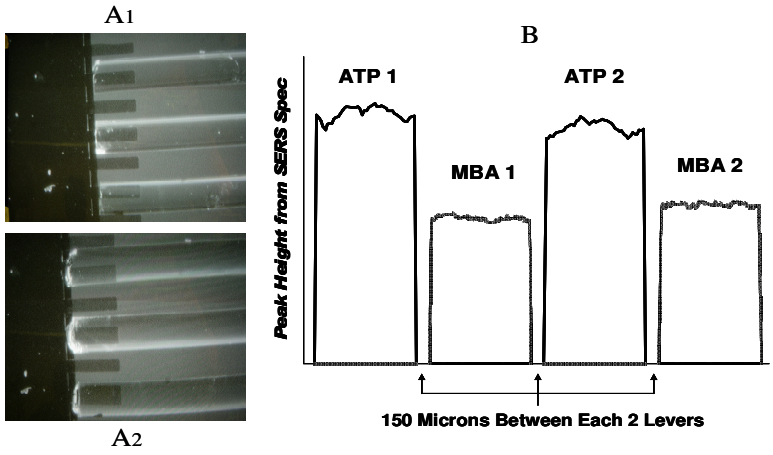

Figure 11. The ability to differentially functionalize adjacent cantilevers in a MCA is demonstrated using a SERS approach. A silver island film (~ 10-15 nm average thickness) was created on the MCs, then the surfaces were functionalized with two different aromatic, thiolated compounds (ATP & MBA). Subsequently, the MCA was spatially scanned under the objective of a Raman spectrometer and a prominent SERS band for each compound plotted versus displacement.

described above. Figure 11B shows the intensity of two different Raman bands specific for ATP (1010-1050 cm^{-1}) and MBA (1055-1095 cm^{-1}) as the instrument scanned laterally across four cantilevers in the array.

The experiment not only confirms that the cantilevers are differentially coated with ATP and MBA, but that the coating is fairly uniform across the width of the cantilever surface and there is no cross-contamination. While MCA sensing and this SERS experiment were performed with distinctly different instrumental arrangements and different cantilever metallic coatings, in principle it should be possible to add the SERS component to MCA measurements directly, perhaps even using the VCSEL radiation for Raman excitation. In fact, in unpublished work, we have observed that DA surfaces exhibit some SERS activity with visible excitation.

3.3.3 Sensor Response and Calibration Performance

To better characterize sensor performance, calibration studies were carried out. The MCA response to calibration experiments was measured for each of the six metal ions included in the study. Table 3 includes the slope of the calibration curve, r-squared value, and relative standard deviation for each of the six metal ions. The MCA sensor demonstrated limits of detection as low as 10^{-8} M based on 3σ of multiple injections of 8.0×10^{-7} M copper chloride solution divided by the slope of the copper chloride calibration plot.

3.3.4 Selectivity

The purpose of creating a sensor array based on this ligand approach is to impart a greater degree of distributed selectivity to the system. Arrays of RPs can be

Phase	MP			AET			MPA			Cyst		
Metal	Slope	R Squared	RSD	Slope	R Squared	RSD	Slope	R Squared	RSD	Slope	R Squared	RSD
CuCl2	0.0069	0.9578	9.02	0.0104	0.9343	11.24	0.0091	0.9979	9.92	0.0079	0.9373	12.35
CoCl2	0.0046	0.9698	8.94	0.0049	0.9577	9.97	0.0043	0.9039	10.42	NA	NA	11.64
CsCl	0.0022	0.6635	11.14	0.0024	0.9236	12.48	0.0214	0.8797	10.89	NA	NA	9.95
LiCl	0.0033	0.9255	10.68	0.0037	0.9333	12.32	0.0164	0.9736	12.63	0.0057	0.9114	9.02
FeCl3	0.0018	0.9712	4.3	NA	NA	5.67	NA	NA	4.71	0.004	0.9607	4.29
AlCl3	0.0041	0.8878	10.24	0.0042	0.9997	10.13	NA	NA	10.78	0.0023	0.7668	9.58

Table 3. The slope, r-squared value, and RSDs for the response to the MCA to three injections of each metal ion at five different concentrations including (1.6×10^{-7}, 8.0×10^{-7}, 8.0×10^{-6}, 2.0×10^{-5}, and 1.0×10^{-4} M).

designed to incorporate a range of analyte-phase interactions (e.g. dipole, van der Waals, hydrogen bonding, electrostatic, coordinate covalent bonding). Each RP in the array may be designed to utilize one interaction more so than the others. The diverse range of analyte-RP interactions in turn provides diversity to the sensor responses. The advanced processing capabilities of pattern recognition algorithms can then be applied to aid in interpretation of the sensor array response. Rather than a high degree of selectivity between a very specific analyte-RP interaction (e.g., Bioaffinity or chelate metal interactions), that generally involves large binding constants and a lack of reversibility, differential selectivity has been imparted to the system through the approach applied herein. In this paper, electrostatic and coordination analyte-phase interactions were taken advantage of by each monodentated RP. However, the ligand functionality for each RP was altered (distributed among the various MCs in the array), effectively changing the interaction of the RP with each metal ion. Selectivity studies were carried out to determine the diversity of response signature of each analyte. Responses to different concentrations of each analyte were measured for all the RPs in the array. Figure 12 demonstrates the diversity of response from metal ion to metal ion. No two response patterns are extremely similar to each other. This apparent response diversity bodes well for metal ion classification via pattern recognition algorithms.

3.3.5 Classification

The classification (metal ion identification) accuracy of the MCA sensor was determined using a leave-one-out cross-validation scheme on the ICA generated

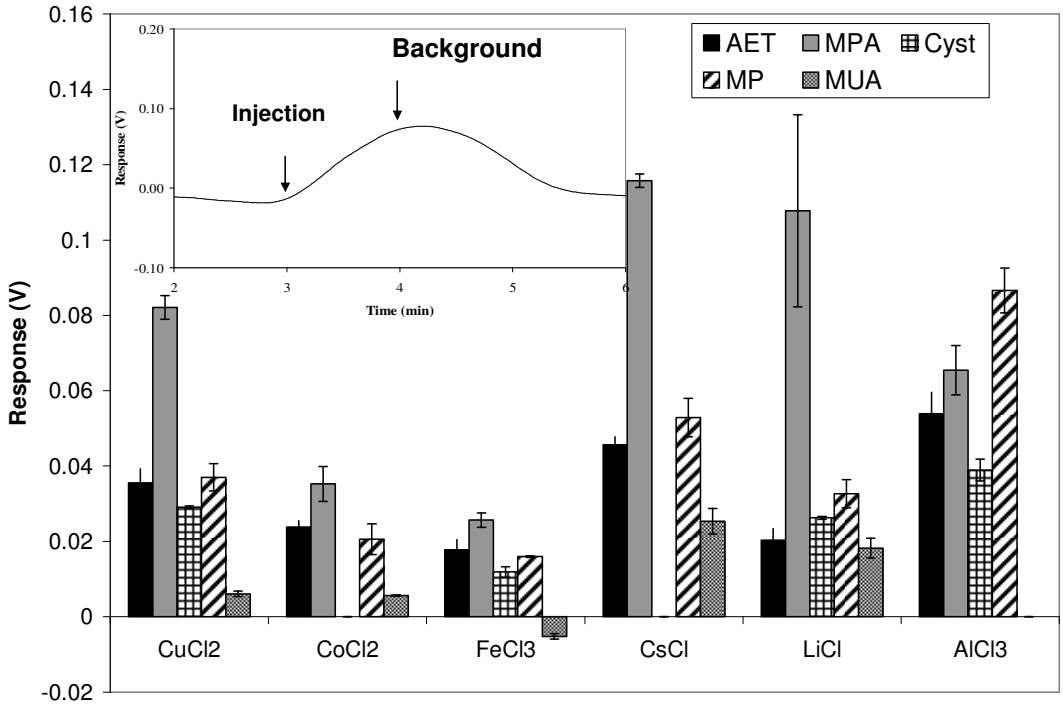

Figure 12. The response diversity to each metal ion is demonstrated in the selectivity plot. In these experiments, 0.01 mM solutions of each metal ion were injected. The insert shows a representative entire response profile of a mercaptopropanol coated cantilever to 0.01 mM Cu^{2+}. In this work a 1 mV response corresponds to 1 nm MC tip deflection.

features. For each trial, a one-against-one SVM multi-classifier was trained using all the remaining trials. The experimental trials consisted of triplicate injections of five concentrations (range of 10^{-4}-10^{-7} M) of each analyte. One of the concentrations in the middle of the range was repeated in triplicate for a total of 18 trials for each metal ion analyte. Each trial contained 12 data sets, one for each cantilever (even though some of the cantilevers were redundant or DA blanks). Thus for each trial, the SVM is trained blind to that particular one-out-of-eighteen trial. Once the SVM is completely trained the trial that was removed from the training can be tested and classified. The generalized prediction rate for each analyte is the fraction of times each trial was classified correctly from a blindly trained SVM.

The generalized prediction rate is a powerful measurement of how much informational content is generated from the sensor array for each analyte, and these generalized prediction rates are given in Table 4. It can be seen in this table that the sensor array is responsive to Al^{3+}, Cs^{+}, Fe^{2+}, and Li^{+}; producing enough information that these metal ions can successfully be identified at rates approaching 90%. However, this is not the case for the doubly charged cations Co^{2+} and Cu^{2+} where the generalized prediction rates are considerably less significant. For example, the Cu^{2+} was misclassified half the trials. Improvements in classification may be realized with improved feature extraction methods and as the library of experimental results for this sensor array builds, providing increased information about the dynamical range and details for each analyte. The fact that the pattern recognition incorporated the entire concentration range, including the concentrations close to the LOD where responses

Tested Analyte	Predicted Fraction for each Analyte					
	$AlCl_3$	$CoCl_2$	$CsCl$	$CuCl_2$	$FeCl_3$	$LiCl$
$AlCl_3$	0.8889	0	0	0.0556	0.0556	0
$CoCl_2$	0	0.6111	0.0556	0.2222	0.1111	0
$CsCl$	0	0.0556	0.7778	0.0556	0	0.1111
$CuCl_2$	0.0556	0.2222	0.0556	0.5000	0.1111	0.0556
$FeCl_3$	0	0.1667	0.1111	0	0.7222	0
$LiCl$	0	0	0.1667	0	0	0.8333

Table 4. Generalized prediction rates for each analyte using leave one out cross-validation of one-against-one SVM multi-classification with ICA feature extraction.

were less reproducible, underscores the power of this approach to accurately classify unknown analyte injections.

In summary, the advantages afforded by configuring MCs in an array format functionalized for differential selectivity is demonstrated for the first time. An ability to uniquely functionalize the individual cantilevers in arrays is verified by a spectroscopic approach. Sensor performance is optimized through altering parameters related to the underlying nanostructured DA layer. The optimal DA layer for sensing was shown by various surface characterization methods to be related to increasing amount of thiol ligand bound to the sensing surface, while also limiting overall cantilever thickness. At optimal conditions the MCA demonstrated limits of detection as low as 1×10^{-8} M. Selectivity experiments yield response signatures that appear unique to the metal ions tested and, when used in conjunction with pattern recognition algorithms, provide a good ability to classify each metal ion even with limited training sets.

CHAPTER 4: DIFFERENTIATING, RESPONSIVE PHASE COATED MICROCANTILEVER ARRAY FOR LANDFILL SILOXANE SAMPLE SENSING

Chapter 4 is an adaptation of a research article *Analytical Chemistry* **2009**, 81, 2575-2580. This article developed a promising way to facilitate in-field detection of siloxanes in landfill gas using a RP-coated MCA. The MCA was nanostructured with DA phase and subsequently coated with 7 RPs. Distinctive response pattern was obtained when the MCA was exposed to specific siloxane in a realistic matrix, with a LOD comparable with that of GC/MS reported by other researchers.

4.1 Introduction

Due to stringent environmental standards and security regulations in many countries of the world, detection of VOCs at trace levels from industrial waste [139], environmental chemical vapors [140], and chemical warfare sources [141] has presented significant analytical challenges. In order to address issues related to selectivity, repeatability, sensitivity, linearity, interferent response, calibration and drift, current research is motivated in material science[142, 143] (directed toward the development of multiple RPs), various sensor measurement strategies (hybrid sensor arrays [144, 145] static and dynamic measurements [146], etc.) and signal processing algorithms (mutli-variate statistical analysis [147, 148], pattern recognition methods [149-151], etc.).

A modern challenge to the analysis of VOCs is derived from landfill gases. Landfill gas produced during the decomposition of organic materials in municipal

waste sites has potential toxicological significance as a contributor to greenhouse effects [152], explosion potential [153], and annoying odors [154]. Owing to the scarcity of traditional natural energy worldwide, it has become important to identify and tap new energy sources for industrial and transportation purposes. Recognizing that the aforementioned detrimental characteristics of landfill gases can be turned to advantages, developed countries have made an increase use of landfill gas, of which methane composes more than 50%, as a new fuel resource [155]. However, the landfill gas is usually contaminated with volatile siloxane compounds, formed from decomposed waste silicon containing organic compounds (e.g., those found in shampoos, tooth paste, silicon oils, etc.), which will form silicon dioxide when they are burned. If the landfill gas containing siloxanes is utilized as fuel, there will be an increase abrasion of gas combustion engines due to silicon dioxide residues forming on surfaces and this leads to loss of engine efficiency. Hence, detection and removal of siloxanes has become a prerequisite to use original landfill gas as fuel and some attempts to accomplish this goal have already been carried out [156].

A real challenge to analytical researchers lies in developing methodologies that are sensitive enough to recognize multiple siloxanes usually present at trace levels in landfill gas. The only reported technique for its trace-level detection in this application has been GC/MS [157,158], but this technique is relatively expensive and also has some limitations for in-field analysis. Fortunately, increasing effort has been spent on the study of inexpensive and portable chemical gas-sensors applied to the detection of VOCs, including multi-sensor arrays with distributed partial selectivity that are

employed in conjunction with chemometric pattern recognition techniques [159, 160]. Specific to our work, during the past several years sensor arrays based on MC transducers have demonstrated advantages [2, 35, 107, 117, 161] over some other comparable sensors such as quartz crystal microbalance or surface acoustic wave devices. These advantages include superior mass sensitivity, small dimensions, and very low cost.

Our previous studies [162, 163] mainly focused on the design of MC sensors in which weak chemical or biochemical stimuli could be converted into mechanical responses with very high efficiency. We have realized high response gain by nanostructuring the active side of the MC. This was most commonly accomplished by depositing an alloy of gold and silver and then preferentially chemically oxidizing the Ag to form a highly granular Au "DA" surface [162]. This surface has much higher surface area and also supplies 3-D obstacles compared to smooth-surface MCs [162-164], which can enhance analyte interactions with RPs deposited on the DA surface and provide better surface stress modulation.

It has been shown that MCs fabricated in different ways have utility for gas phase sensing [151, 165-169]. In the work reported herein, thin films of seven different RPs were vapor deposited onto the DA surface of commercially available MCs to make a MCA for siloxane sensing. Four standard gas samples with different trace amount of siloxane dissolved in helium and a simulated realistic matrix containing methane, carbon dioxide, nitrogen and water vapor were tested and the MCA was showed to supply a characteristic response signature for each siloxane sample. Calibration

plots were obtained that produced limits of detection (LODs) that in some cases were very close to those [158] reported for GC/MS. Calibration of the developed MCA can be performed by standard addition methods [170, 171] if necessary, which is particularly useful at compensating the effects of matrix on the responses of the measured siloxane samples when the effects can not be neglected. However, in our present work, no distinctive differentiation was observed between the helium and matrix siloxane samples in terms of the recognition performance and sensitivity, and the long term stability of the MCA is also demonstrated. The work reported herein represents an excellent example of how nanomechanics based on MCAs can aid in areas of energy and environmentally related significance.

4.2 Experimental

4.2.1 Chemicals and Materials

Information of MCs and metals can be found in the previous chapter. RPs for MC coatings included heptakis(6-O-tert-butyldimethylsilyl-2,3-di-O-acetyl) -β-cyclodextrin (AcβCD), tetrabutylammonium p-toluenesulfonate (TBATS), poly(ethyleneimine) (PEI), poly(diphenoxyphosphazene) (PDPP), 4-tert-butylcalix[6]arene (Cal-6), 4-tert-butylcalix[6]arene (Cal-4) and squalane (Squ). AcβCD, TBATS and Squ were obtained from Sigma-Aldrich, PEI and PDPP were purchased from Scientific Polymer Products (Ontario, NY), and Cal-6 and Cal-4 were acquired from Lancaster (Pelham, NH). Standard siloxane reagents included pentamethyldisiloxane (PMDS), hexamethyldisiloxane (HMDS), octamethyltrisiloxane (OMTS) and decamethylcyclopentasiloxane (DMCPS). PMDS and OMTS were

obtained from Oakwood Products (West Columbia, SC), while HMDS and DMCPS were purchased from TCI AMERICA (Portland, OR). All chemicals were above 99% in purity and used as received.

4.2.2 Instrumentation and Sample Preparation

Background gas was controlled at a certain flow rate by a multi-tube flow meter (Cole-Palmer Co.). Especially for matrix sample analysis, due to a more complex background in which the volume percentage of each gas component was fixed, a special flow system was set up to control the flow rate of each. As showed in Figure 13, gas flow streams of CH_4, CO_2 and N_2 were controlled by the multi-tube flow meter to be at a constant flow rate converging into a stream in the ratio (CH_4 : CO_2 : N_2 = 10 : 1 : 9). The mixture stream was then saturated with water vapor to produce a simulated matrix background gas flow. Because of the potential detrimental affect of water vapor on RPs, a desiccator filled with *Dryright*^{TM} was assembled into the flow system to dry the matrix background gas before it flowed across the RPs-coated nanostructured MCA. The MCA was mounted in a home-made flow cell having a total volume of approximately 100 μL, with an inlet and an outlet port. The flow cell was placed in an optical system and contained a window to facilitate the observation of MC deflection. The same VCSEL system was used as described in the previous chapter for data acquisition.

The background gas collected from the outlet of the flow cell into the *Tedlar* sampling bag (SKC South Inc) was used as the solvent to dilute pure siloxane vapor into any needed siloxane samples. Siloxane vapor was extracted from a headspace vial

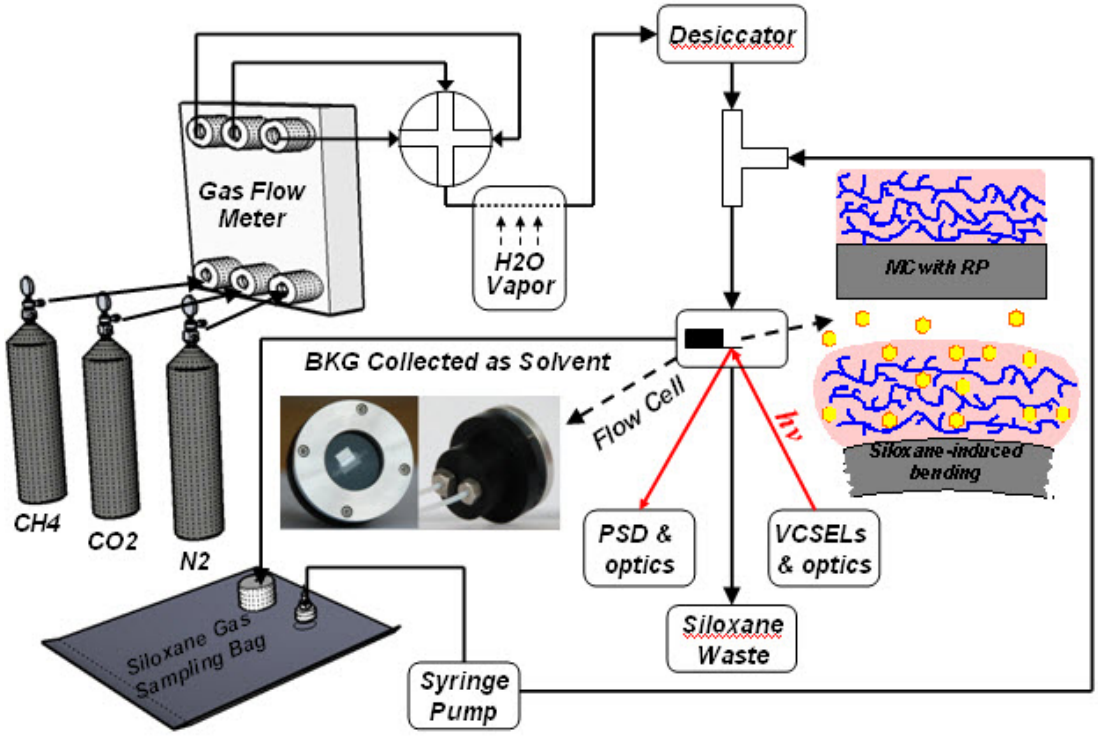

Figure 13. Schematic representation of the instrumental set-up: matrix background flow generation, diluted siloxane sample delivery and MC deflection monitoring. The insert picture shows a front view of the flow cell with the MCA mounted inside.

with an analyte syringe (Fisher). The requisite amount of headspace vapor for preparing a siloxane sample at certain concentration level can be calculated with the equation (PV = nRT) in which *P* is vapor pressure of the siloxane at ambient temperature *T* in *Kelvin* and *V* is the headspace volume in the vial. The number of moles for the siloxane, *n*, can be calculated thereafter (R is a constant). Vapor pressure value of each siloxane could be deduced from the *Antoine* Equation (Eq. 8), one of the most wildly used equations to estimate the temperature dependent vapor pressure of pure organic liquids [172-175].

$$\ln P_{vp} = A - \frac{B}{T + C} \qquad (8)$$

P_{vp} is the vapor pressure at certain temperature *T*, while *A, B* and *C* are constants for specific siloxane. Despite poor performance to some organics such as fatty acid esters [176], *Flaningam* [177] has provided the experimental vapor pressure value perfectly fitting with the *Antoine* Equation for those linear, cyclic and branched methyl siloxane liquids with low molecular weight. Thus, reliable vapor pressures of the siloxanes could be obtained in our present study.

4.2.3 Cantilever Modification and Coating.

DA nanostructured modification and RPs coating of the MCs were both accomplished using a PVD procedure which was carried out in a vacuum chamber with a resistively heated source at a pressure of approximately 1×10^{-6} torr [163, 164, 169]. Tungsten boats and alumina crucibles with thermal heaters were used for evaporation of the metals (Cr, Au and Ag) and the RPs. Deposition rate and resulting coating thickness were monitored using a quartz crystal microbalance. Initially 8 nm of

Cr was deposited onto cleaned MCs followed by 15 nm of Au. A 100 nm thick Ag/Au composite film was then created by co-deposition of Ag and Au in equal proportion. To create DA nanostructured surfaces from the Au/Ag film, the silver was etched out of the composite film by placing the cantilevers in an aqueous solution of 0.2% w/v $HAuCl_4$ for about 3 minutes. The cantilevers were then rinsed with copious amounts of water after etching [162]. Thereafter, films of RPs were vapor deposited onto the DA surface of the MCs. A slit with ~150 μm width was used to selectively expose only one lever to the organic vapor so that the vapor could be deposited onto only one lever at a time without cross contamination. The VCSEL radiation was focused onto 12 MCs coated with seven different RPs. Some levers were duplicates and some others were coated with the same phase but at different thicknesses.

4.2.4 Data Acquisition

Data acquisition using Labview program was the same as previous chapter. Throughout the experiment, background gas (either helium or matrix) was maintained at a constant flow rate of 4.0 mL/min, controlled by a mass flow meter connected to the outlet of the flow cell. A flow of siloxane sample was injected into the background gas stream via the tee shown in Figure 13 by a syringe pump at a rate of 0.8 mL/min. Injection lasted for 60 seconds, followed by a 180-second background gas flow. For response time studies, a six-port injector with 1 mL injection loop was used instead of the syringe pump for siloxane sampling, and injection was followed by a 120-second background gas flow.

4.3 Result and Discussion

All the parameters for DA surface modification have been optimized in our previous work [150] such as the thickness of nanostructured film, the relative amount of Au and Ag contained in the DA film, and dealloying duration time. It has also been verified by FTIR spectra and gel permeation chromatography that the RPs used can be vapor deposited without much structural change [169]. The conversion of analyte (siloxane compounds herein) induced swelling of the RPs into surface stress and bending of the cantilever is inefficient if slippage of the phase occurs. A major benefit of our DA surface, with previously determined root mean square roughness of about 35 nm [162], is that thin films of RPs in the range of thicknesses used herein are stabilized from slippage [163]. A depiction of siloxane induced MC surface changes is seen as an insert in Figure 13.

4.3.1 Calibration Performance and Sensitivity

MCA sensor performance can be summarized with a calibration study. Figure 14A shows a calibration curve for 60-second injections of 0.1, 0.25, 0.5 and 1 ppm of siloxane in the matrix environment. The magnitude of response increased with the concentration of siloxane in a linear fashion (Table 5). Moreover, our prior work [5, 71, 162, 163] has shown that the calibration plots were generally linear for two or more orders of magnitude while coefficients of variation for measurements using a given MC-phase were generally 10% or better. In the present study, a LOD as low as 0.017 ppm was obtained based on 3σ of multiple injections of 0.25 ppm of siloxane sample divided by the slope of the corresponding calibration plot [178].

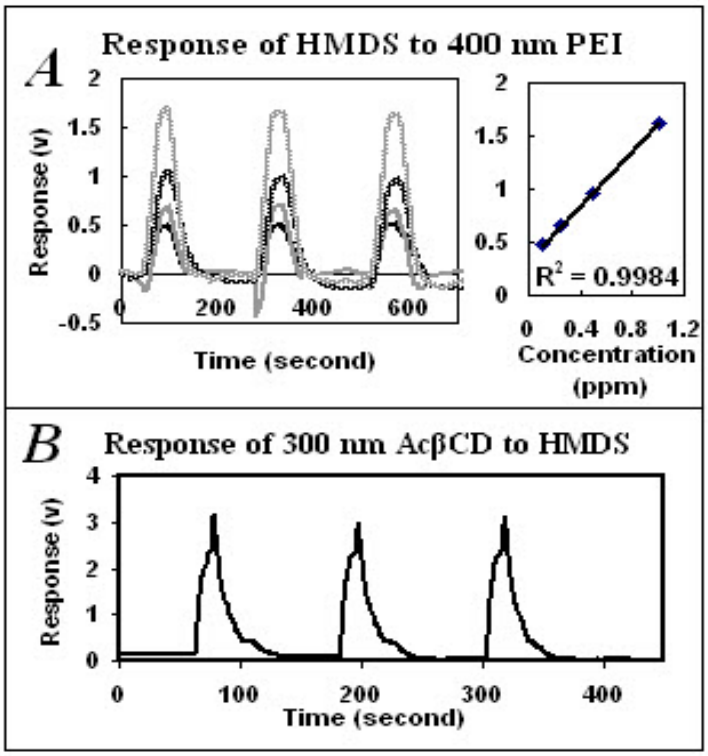

Figure 14. **(A)** HMDS response profiles from the cantilever having 400 nm PEI RP, obtained by 60-second injections of HMDS with a syringe pump in triplicate, as well as the corresponding calibration plot; **(B)** 0.5 ppm HMDS response profiles obtained by three consecutive injections of HMDS samples with 1 mL injection loop.

	r-Square	LOD (ppm)	CV (%)
PMDS	0.8819~0.9940	0.050~1.5	2.11~8.88
HMDS	0.8337~0.9995	0.048~0.17	1.65~13.5
OMTS	0.7527~0.9920	0.047~1.1	2.63~17.8
DMCPS	0.9799~0.9811	0.017~0.083	0.57~6.53

Table 5. Results of calibration study in terms the range of calibration plot *r*-squared value, LOD and CV (coefficients of variation) obtained from all the RPs on the MCA to each of the four siloxanes.

For this MC sensor in signaling the presence of siloxanes, performance is also characterized by response and recovery times. Herein, we define the response time as the time to reach 90% of full-scale cantilever deflection and recovery time as the time for the response signal decreasing from maximum to 10% of full-scale cantilever deflection for our injection protocol. An injection loop with fixed volume (1.0 mL) filled with siloxane sample was used for response time measurement. To ensure high accuracy for response time measurements, the injection loop was overfilled with the siloxane sample and the distance between the loop outlet and flow cell inlet was minimized. Response data are plotted in Figure 14B. Evaluation of response profiles shows the response and recovery times of all the RPs on the MCA to siloxane samples are all less than 15 seconds and 35 seconds, respectively.

4.3.2 Study of Matrix Effect

In real-life sensing applications, the matrix effects vary with chemical and physical conditions such as temperature and humidity in the sensing environment. Water vapor is always present in the realistic landfill gas matrix, but in our present study, we noted that overly-high humidity degraded the responsive function of the MCA. Our experiments showed that RPs coated DA MCs lost almost all response to siloxanes after overnight exposed to water vapor saturated air. Hence, an on-line desiccator was assembled in our flow system to avoid MCA water vapor exposure. Response data of the MCA were compared between wet background flow with desiccator treatment and dry background flow. No distinct deviation was observed between the two response profiles as seen in Figure 15.

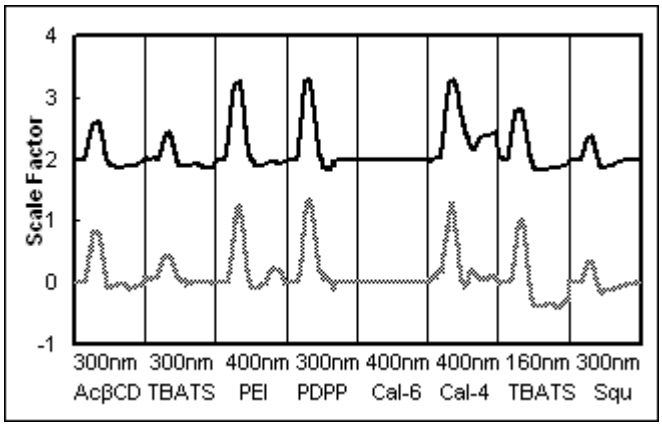

Figure 15. Response profiles of the MCA to 0.5 ppm PMDS delivered into desiccated wet matrix background flow (top) and the matrix background flow without water vapor (bottom).

The discrepancy between the matrix background flow and the matrix sample solvent collected in the *Tedlar* bag was minimized in this work. It was observed that some of the RPs on the MCA responded slightly to injection of the blank matrix sample solvent without any siloxanes. Fortunately, response subtraction of the generated matrix from the siloxane samples yielded an overall response profile that closely resembled siloxane samples in helium, with no significant increase in the LODs or decrease in calibration linearity (Table 6).

4.3.3 Distributed Selectivity

Selectivity studies were carried out to determine the diversity of response signatures between the four siloxane samples. Responses to different concentrations of each siloxane sample were measured for all the RPs coated levers on the MCA. Well designed arrays of RPs should incorporate several different modes of siloxane-phase interactions such as dipole, *Van der Waals*, hydrogen bonding, electrostatic, etc. When this is accomplished, distributed selectivity of the system can be achieved based on the differences in sensor responses provided by a range of siloxane-RPs interactions. Figure 16 demonstrates the diversity of responses of the MCA to each of the four siloxane samples injected in triplicate (details are in the caption). We can easily see that DMCPS has a distinguishable signature response compared to the other three, which is reasonable because cyclic molecules should apply different spatial interactions on the RPs from linear molecules. The other three siloxanes have more similar signatures but are distinguishable. For example, the Cal-6 phase only responded to HMDS, while the response deviation between AcβCD and TBATS (300

	Matrix Environment		**Helium Environment**	
	r-Square	LOD (ppm)	r-Square	LOD (ppm)
PMDS	0.9940	0.072	0.9946	0.061
HMDS	0.9713	0.048	0.9916	0.097
OMTS	0.9920	0.047	0.9833	0.021
DMCPS	0.9799	0.017	0.9858	0.022

Table 6. LOD & r-square obtained in matrix environment compared with those in helium environment from the same RP coated MC.

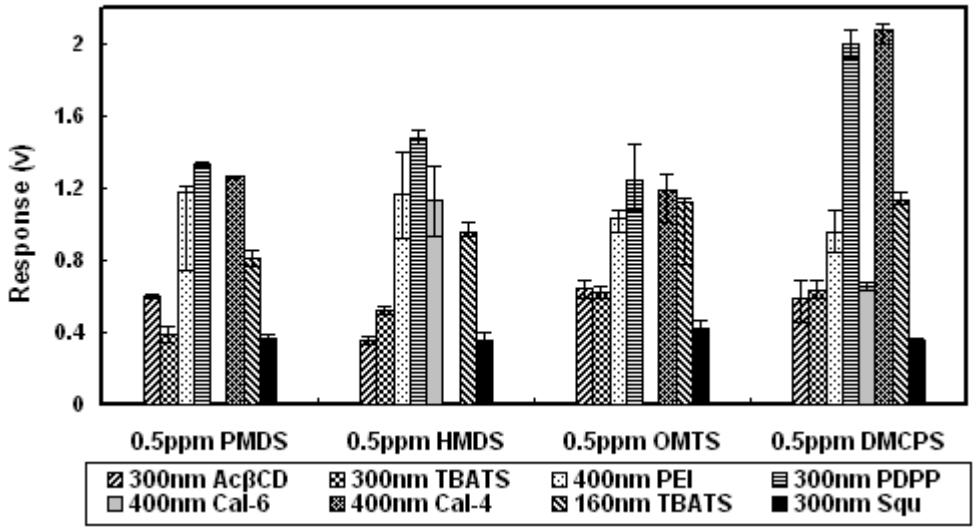

Figure 16. The selectivity plot shows the response diversity to each siloxane for MCA. In these experiments, 0.5 ppm of each siloxane in a matrix environment was injected for 60 seconds in triplicate and the average peak signals are plotted.

nm) is distinct for PMDS but not for OMTS. In prior gas phase work this level of variability in overall MCA response signatures was adequate for classification (identification) of analytes using pattern recognition techniques [151, 179, 180].

4.3.4 MC-to-MC and Long-Term Reproducibility

Three pairs of DA cantilvers on the MCA were coated with the same RPs in the same (AcβCD and PEI) and different (TBATS) thickness respectively. Figure 17 shows that good responsive lever-to-lever reproducibility was observed if the thickness of the coated RPs were the same. Otherwise, distinct deviation was observed: the DA cantilever coated with a thinner TBATS phase gave a larger response than thicker TBTAS phase (Figure 15). In general, the magnitude of signals scales with thickness [163] so this was not expected.

Response profiles for the seven RPs on the same MCA to the same four siloxane samples obtained in the matrix were recorded 5 weeks after collecting the initial response profiles. Using 1 ppm OMTS as an example, Figure 18 illustrates the excellent reproducibility over a 5 week time period for MC responses. It should be noted that during the 5 week period the array was in continuous use. Considering that VCSEL-MCA systems usually undergo calibration with standards on a frequent basis, the reproducibility was pleasing given that no unique calibration or normalization work was performed. However, the array to array reproducibility was not satisfying, which may be due to array to array size and stress variations. Note that MCs on different chips usually show an obvious variation in the resonance frequency of higher than 15% within the same purchased batch. Also, the conditions of vapor deposition of

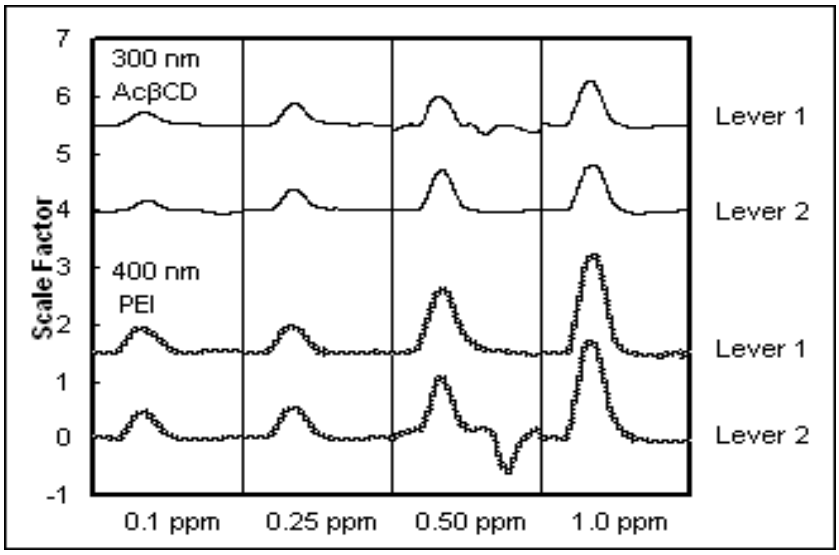

Figure 17. Response profiles of two MCs coated with identical RP: 300 nm AcβCD and 400 nm PEI respectively, exposed to 0.1, 0.25, 0.50 and 1.0 ppm DMCPS for 60 seconds.

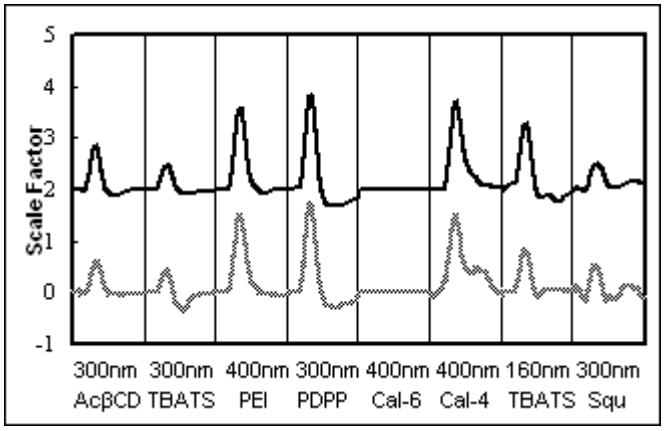

Figure 18. Comparing the response profiles of the MCA to 1 ppm OMTS (top) in matrix environment with those of an identical measurement obtained after 5 weeks of use (bottom). Each grid corresponds to a 280 second response.

RPs were not precise enough for array to array duplication. Hence, each MCA should be uniquely calibrated.

4.3.5 Potential Applicability to Realistic Landfill Sample Analysis.

The apparatus depicted in Figure 13 is utilized to generate a flow of gas mixture mimicking real landfill gas background, which may not be the same as normal atmospheric conditions. When adapted for in-field use it is envisioned that the apparatus will actually be simplified. The cumbersome gas cylinders and flow meter will be replaced by a simple gas pump that will sample and deliver ambient landfill gas to the flow cell. In addition, the tee in the figure would be replaced by a multi-port valve, for example an HPLC six port injector, that allows one to switch between flow through an active carbon adsorber [181] or gas permeation membrane [182] to scrub the siloxanes (if present) from the stream and a path that bypasses the scrubber. In this manner the valve would permit toggling between landfill gas with and without the siloxanes to effectively make siloxane or siloxane-void injections.

In summary, we have developed a new approach for detecting trace siloxanes in matrix landfill gas sample with RP coated MCAs. The seven RPs created a unique recognition pattern for each siloxane and the RPs exhibited stability for a period of more than a month. LODs as low as 0.017 ppm were obtained from the siloxane calibration plots. A matrix effect study was carried out and based on simple background subtraction a comparable LOD was obtained for siloxanes in both a realistic matrix and inert helium environment. The high sensitivity of the MCA combined with a rapid response time renders our approach very competitive to GC/MS

which has previously been used for trace siloxane analysis. However, our method is much less expensive and requires less power. The small dimensions and portability of our setup will make it promising to facilitate in-field siloxane analysis, which can be expected to improve the cost effectiveness of harnessing landfill gas as an energy source.

Vapor deposition of gold and silver usually causes a lot of waste because most of the evaporated metal will not be coated onto the MCs. What's more, the deposition protocol needs to be carried out under vacuum and any mild leaking of the vacuum system will lead to poor adhesion of DA phase to the MC surfaces. The next chapter will discuss a newly developed nanostructured MC sensor which is stable, cheap, and applicable to both chemical and biological sensing.

CHAPTER 5: ALUMINIUM OXIDE NANOSTRUCTURED MCA FOR NANOMECHANICAL-BASED SENSING

Chapter 5 is an adaptation of a research manuscript submitted to *Langmuir*. In this manuscript, uniform layers of aluminium oxide nano-particles (AONP) were chemically immobilized on MC surfaces. Optimization studies were carried out for better surface uniformity and higher surface area of this new phase. One MCA was functionalized with three alkoxysilanes for VOC sensing, and a second MCA was functionalized with two different immunological receptors for biological sensing. Highly selective response and good sensitivity were obtained from both of the MCAs. The controlled, variable chemical natures of the MC surfaces were validated by FT-IR and fluorescence microscope images.

5.1 Introduction

As one of the most common micromechanical devices, MCs have been extensively applied in chemical [67, 164, 183, 184], biological [169, 185-186] and physical [187] sensing areas during the last decade or so. Significant efforts have been spent to achieve higher sensitivity using this sensing technology [184, 185, 188-192]. In general, cantilevers intended to be used as sensors are modified so that one side can preferentially absorb or adsorb the target analyte [107]. Enhanced surface area of this side is always advantageous for higher sensitivity, because the number of analyte-binding sites on the cantilever is substantially increased. Nanostructured surfaces and coatings, such as surface-immobilized nano-scale colloids, are now recognized as one of the paradigms for increasing surface area of the active side of

MCs for better sensitivity [162, 163, 164, 184, 193, 194]. Earlier studies have demonstrated that up to two orders of magnitude increase in cantilever responses can be obtained when receptor molecules are immobilized on nanostructured instead of smooth, coated MC surfaces [69, 163].

Currently, to prepare a nanostructured surface, MCs are usually coated with a layer of sensing materials such as metal [195], polymer [196, 197], silicon compounds [198, 199] and carbon nano-tubes [194], followed by further treatment if necessary to make the layer more roughened or porous [163, 164, 200]. During recent years, there is an uptrend to modify MCs with metal oxides for better sensitivity due to their specific properties [201-203]. The metal oxide layer was usually obtained through either direct depositing [204, 205] or oxidizing the deposited metal layer [206, 207] to create a nanostructured surface. Although these oxide phases had an increased surface area, the lack of functional groups having more intricate structures on the surface confines the range of their applications. Being aware of that restriction, some attempts have been initiated for gaining more versatile surfaces by grafting a linker compound, such as, alkoxysilane, onto the surface of the metal oxide phases for MC sensors [208-210].

Inspired by the utilization of alkoxysilanes [208-210], a new method for nanostructuring MCs with metal oxides was developed in the work reported herein. Previous reports [211, 212] have shown that aluminium oxide could be functionalized by alkoxysilanes, so we chemically immobilized tetramethoxysilane (TMOS)-modified AONP onto the MC surfaces through cross-linking, to form a stable and uniform layer of AONP. Optimization work was performed to make a high density layer of AONP

uniformly dispersed on the MC active surfaces. This layer can be subsequently functionalized with other alkoxysilanes with a variety of surface active functional groups (Figure 19). To our knowledge, no studies have been carried out before on modifying aluminium oxide phase coated on MC surfaces for detecting specific target analytes. Furthermore, in order to impart an enhanced selectivity to the AONP-modified MC sensor by earning diverse response patterns for various target analytes, MCs on the same chip were differentially functionalized with various receptor phases to create a true MC sensor array. This MCA was prepared by immersing MCs in different solutions for functionalization using a capillary array setup (Figure 20) as described in detail elsewhere [150]. As previously demonstrated by the Sepaniak group [110,150,151,169] and other researchers [213-215], differentially functionalized MCAs can impart a good degree of distributed selectivity to a system. Moreover, the advanced processing capabilities of pattern recognition algorithms could be utilized for differential selectivity, aiding in the interpretation of the sensor array responses and facilitating identification of analytes having similar structures [150,151].

One MCA was prepared by differentially functionalizing MCs with three different alkoxysilanes to form a SAM of recognition sites on each MC surface, for VOC sensing in gas phase. In order to improve sensitivity, both the component of the alkoxysilane solution and the MC immersion time in the solution were optimized in advance. The MCA was exposed to samples composed individually of four VOC headspace vapors, and a highly selective response signature for each VOC was easily

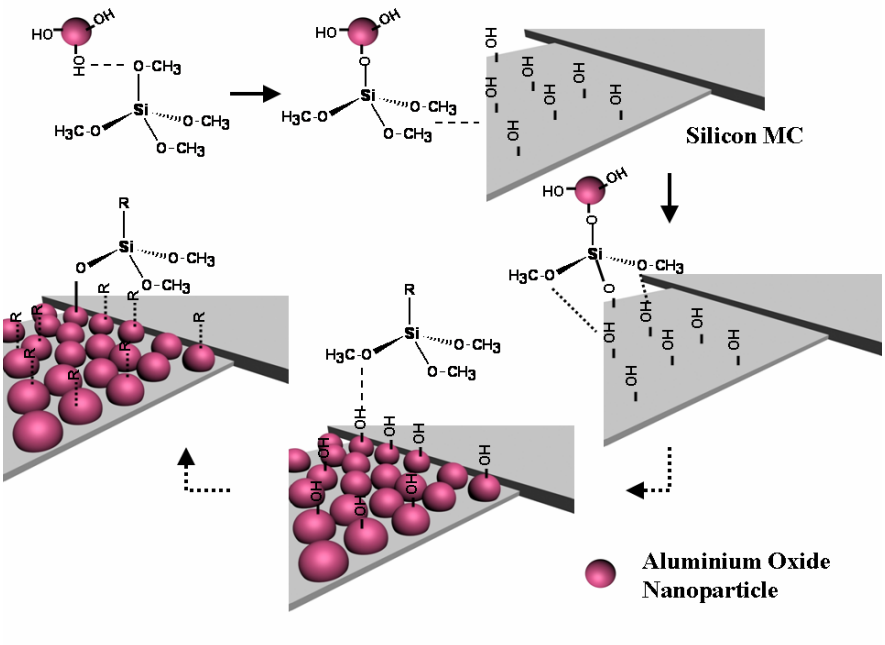

Figure 19. Scheme of nanostructuring MC surface with AONP and then functionalized with alkoxysilanes.

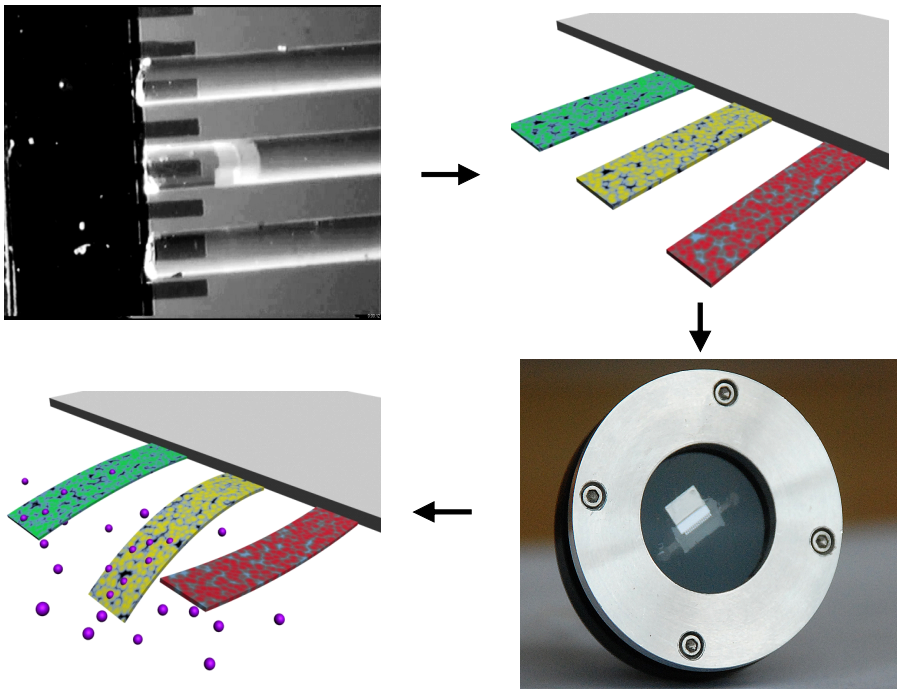

Figure 20. AONP-nanostructured MC chip were differentially functionalized with a capillary array filled via capillary action with various alkxoysilane solutions (the middle capillary is in process of filling). The functionalized MCA was then loaded in a low volume (~5 μL) flow cell and demonstrated diversity in deflection from lever to lever when exposed to the same analyte.

obtained. A LOD down to 0.13 μg/mL was derived from the calibration plots with good and respectable r-squared and CV values. Long-term and lever-to-lever reproducibility of the MCA's response to the same analyte was also demonstrated. A second MCA was prepared for biological sensing in liquid phase. In this array, anti-immunoglobulin G (anti-IgG) and anti-biotin were immobilized onto two MCs as bio-receptors with the capillary coating manner, with the same procedures reported in our previous works involving MC bio-sensors [216], except using (3-aminopropyl)trimethoxysilane (APTMS) to produce a SAM of amino groups. Although no optimization work was performed, a true immuno-based MCA was created with biological discrimination capabilities in this work.

5.2 Materials and Methods

5.2.1 Reagents and Materials

The same MCs, deposited metals, and flexible capillaries as the previous chapters were used. AONP (99.97 %, 20-30 nm) were purchased from NanoAmor (Houston, TX) and dried at 120 ºC for at least 24 h prior to any use. Alkoxysilanes and glutaraldehyde (GA) were obtained from Sigma-Aldrich. All biological reagents were also obtained from Sigma-Aldrich except Alexa Fluor 633 goat anti-hIgG which was purchased from Invitrogen Co. (Carlsbad, CA). All the other chemicals used in our study were purchased from either Sigma-Aldrich or Fisher. All the chemicals were purchased at highest available purity and used as received. Water used to prepare solutions was obtained from a Barnstead E-Pure water filtration system.

5.2.2 MC Modification

The MCs were modified by spin coating a slurry prepared with AONP, TMOS and absolute ethanol. Initially, 0.02 g AONP was homogeneously dispersed in 5 mL absolute ethanol by sonicating for 1 h. Then 0.1 mL TMOS was added and the sonicating was maintained for another 1.5 h before the slurry was ready to use. Before spin coating, the MCs were boiled in piranha solution (V_{H2SO4} : V_{H2O2} = 7 : 3) for 1 h. 50 μL of the slurry was spin coated onto the surface of the MC chip at the rate of 6,000 rpm and the rate was held for 30 s to evaporate all the ethanol. This coating procedure was repeated seven times and the coated MCs were cured in desiccator for at least 12 h.

5.2.3 Modification of AONP-modified MCs

The capillary coating apparatus was used to differentially functionalize AONP-modified MCs (see Figure 20). Detailed information can be found in previous chapters. For VOC sensing in gas phase, three pairs of MCs on the AONP-modified MCA were functionalized with 2 % (v/v) solution of APTMS, octadecyltrimethoxysilane (ODTMS) and (3-Glycidyloxypropyl)-trimethoxysilane (GPTMS) in absolute ethanol one after another, and the immersion time of MCs in each solution was 7 minute, 4 h and 2 h. 2 % (v/v) acetic acid was added in the solutions of ODTMS and GPTMS as a catalyst.

For biological sensing in liquid phase, AONP-modified MC chip was immersed in 2 % (v/v) solution of APTMS in absolute ethanol for at least 4 h [212]. The MC chip was then removed from solution and rinsed with copious amount of absolute ethanol

and dried under nitrogen flow. The formed amino groups on the MC surfaces were derivatized with the cross-linker by immersing the MC chip in 1 % (v/v) solution of GA in water/phosphate buffered saline (10 mM pH 8 PBS) for 3-h incubation and then rinsed with a large volume of 10 mM pH 8 PBS to remove any non-specifically bound GA on both sides of the MCs. The bio-receptors were then immobilized onto the MC surfaces by capillary coating 0.5 mg/mL solution of the receptors in 10 mM pH 7 PBS for 1 h to create a differentially functionalized bio-sensing array, followed by rinsing with copious amount of 10 mM pH 7 PBS.

A 50 nm layer of gold was vapor deposited onto the passive silicon sides of the MCs with a 5 nm layer of chromium underneath the gold for better adhesion. This was performed on the bio-sensing array after AONP-modification but on the VOC-sensing array as the last step. The gold layer can make this side more passive and supply enhanced reflection of source laser to obtain better signal.

5.2.4 Instrumentation

The same capillary coating setup and VCSEL systems as previous chapters were used. FT-IR spectra were collected by performing specular reflectance with a Varian 4100 FT-IR spectrometer. SEM images were collected with a LEO 1525 microscope with a field-emission gun operating at 5.00 kV. A Leica SP2 laser scanning confocal microscope having an Ar ion laser with 488 nm beam and a He-Ne laser with 633 nm beam was used for capturing fluorescence images.

5.2.5 Data Acquisition

For gas-phase experiments, pure nitrogen background gas was controlled at a constant rate of 3.2 mL/min by a mass flow meter. Gas samples were prepared by diluting the headspace vapor of VOCs with nitrogen in either a sample syringe (Hamilton) or a gas sampling bag. The prepared sample was transferred to a sample syringe and injected into the nitrogen stream by a syringe pump at a rate of 0.8 mL/min for 60 second. The injection was followed by another 100 second nitrogen background flow. For liquid-phase experiments, 10 mM pH 7 PBS was used as background with a flow rate of 0.1 mL/min. Analyte were delivered to the flow cell via a system of vessels connected to three-way valves allowing for switching between background and analytes. The injection of analyte lasted for 100 second.

5.3 Results and Discussion

5.3.1 Spectral Characterization of Functionalized AONP-Modified Surface

The IR spectra of plain and functionalized AONP-modified surface are shown in Figure 21. Due to the difficulty of focusing the laser spot onto MCs, silicon wafer with a similar size to a MC chip was modified with AONP and then functionalized. In order to simulate the capillary coating method, the wafer was partially dipped in small amount of solution for functionalization (except Figure 21e and 21f). After the modification with APTMS, either by partially dipping (Figure 21b) or by functionalizing in bulk (Figure 21e), a broad band occurred in the 2850-3050 cm^{-1} region due to the stretching of methylene in the alkylamine group, and another new peak occurred in the 1580-1650 cm^{-1} region due to N-H deformation [217-219]. After

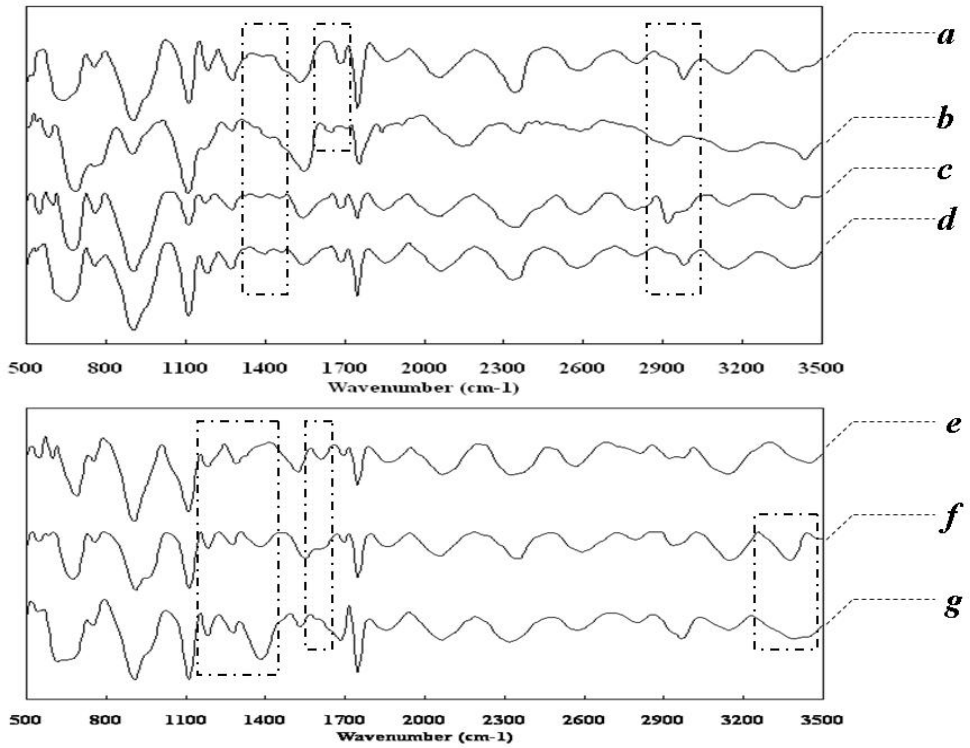

Figure 21. FT-IR spectra of AONP-nanostructured surface (a) and functionalized with APTMS (b), ODTMS (c), and GPTMS (d). FT-IR spectra were also collected while AONP-nanostructured surface was functionalized with APTMS (e) first, then with GA (f) and ultimately with protein A (g).

the modification with ODTMS, one sharp peak was seen in the 2840-2975 cm^{-1} region for C-H stretching in aliphatic hydrocarbons [220,221] while two additional new peaks in the 1350-1500 cm^{-1} region were derived from the deformation of methylene and methyl [217] (Figure 21c). After the modification with GPTMS, due to the deformation of methylene and methine in the epoxide ring, two new bands at 1400 cm^{-1} and 1460 cm^{-1} were observed [217] (Figure 21d). After the APTMS-modified (in bulk) surface was functionalized (in bulk) with GA, a new peak at 1388 cm^{-1} was seen due to C-H rocking vibration in the aldehyde group [217], while the peak at 1620 cm^{-1} disappeared as a result of the reaction between amino groups on the AONP's surfaces and carbonyl groups in GA (Figure 21f). The surface was subsequently functionalized with anti-IgG and accordingly the peak in the 3240-3500 cm^{-1} region became broad due to N-H stretching vibrations (Figure 21g) in peptide bonds [217].

5.3.2 Optimization

Optimization of the sensor's response is influenced by uniformity and density of the functioning sites on the nanostructured surface. However, exorbitantly high density of binding sites may lead to a decrease in sensitivity due to steric hindrance effects.

The prerequisite to make a highly responsive MCA is the uniformity of the surface morphology. Our optimization work focused on five aspects that may influence the uniformity of the AONP modified surface, including the type of solvent, density of the AONP slurry, spin coating times, concentration of TMOS and sonicating time, with evaluations based on the SEM images. In order to evaluate surface uniformity, shorter working distance and Inlens (upper) mode of the LEO 1525 microscope was

applied to collect the SEM images. AONP slurry prepared with ethanol could form a homogeneous film after being spin coated onto silica surface, while aggregates of AONP were obtained if other solvents such as acetone, chloroform or toluene were used. Figure 22A shows the nanostructured surface modified with the optimal manner as explained previously in this chapter. A lower density of the AONP-slurry produced a very sparse coating (Figure 22B), while a higher density caused aggregation of AONP (Figure 22C), both of which resulted in non-homogeneity. 50 μL of AONP-slurry was spin coated each time. Spin coating the AONP-slurry 4 times or 6 times (See Figure 22D & 22E) produced a sparse non-homogeneous layer, while coating more than 8 times led to aggregation of AONP on the surface. The density of the AONP slurry was the primary factor in determining uniformity. In other words, a uniformly nanostructured surface could not be obtained without a specific slurry density, no matter how many times the slurry is spin coated. As a cross-linker, the TMOS concentration is important. If the TMOS concentration is too low then it may not form linkages on all the AONP as illustrated in Figure 22F, while too much TMOS may cause aggregation of the AONP. This can occur due to cross-linking between the AONP as seen in Figure 22G. Sonicating for 1 h produced a homogeneous AONP-slurry before TMOS was added, while sonicating for at least 1.5 h was needed to modify all the AONP. Sonicating for longer than 2.5 h caused aggregation of AONP and led to weak adhesion onto MC surfaces. In summary, the optimized protocol for nanostructuring MCs with AONP involved dispersing 0.02 g AONP in 5 mL absolute ethanol by sonicating for 1 h, adding 0.1 mL TMOS into the slurry with sonication for

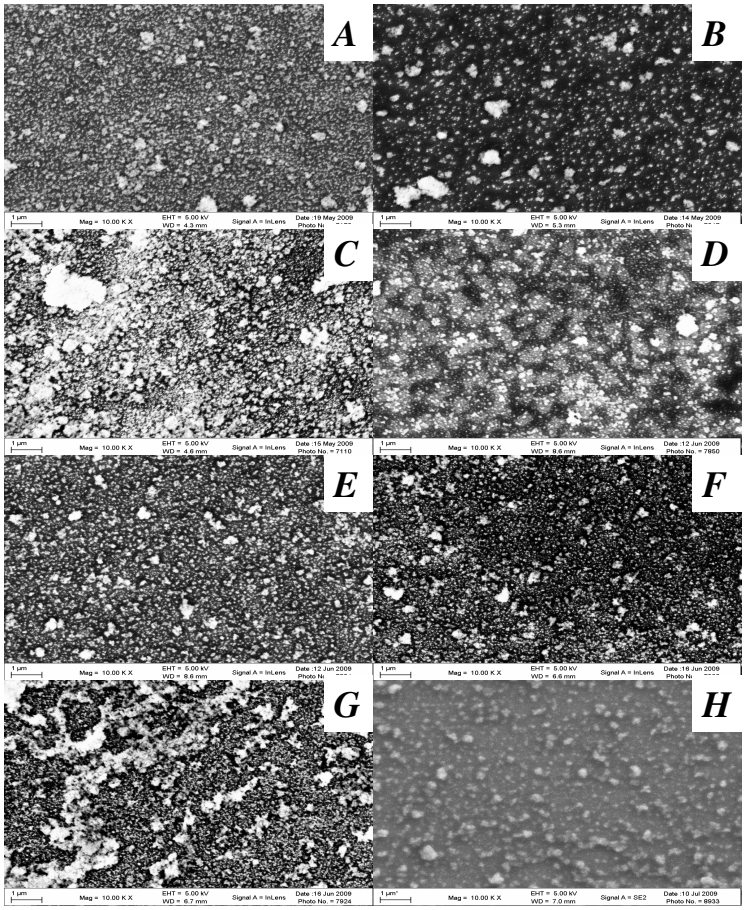

Figure 22. SEM images of AONP-fabricated surface prepared: (A) with the optimized manner, (B) with AONP slurry with density of 0.002 g/mL, (C) with AONP slurry with density of 0.008 g/mL, (D) with the optimal AONP slurry spin coated for 4 times, (E) with the optimal AONP slurry spin coated for 6 times, (F) with AONP slurry modified with 0.5 % (v/v) TMOS, (G) with AONP slurry modified with 5 % (v/v) TMOS, (H) with optimized conditions and then functionalized with GPTMS. All micrographs were collected at 10 K magnification.another 1.5 h, and finally spin coating the slurry onto MC surfaces 8 times, with 50 μL coated with each application.

In order to obtain the highest sensitivity for VOC detection, both the immersion time of MCs for functionalization and the components of alkoxysilane solutions were optimized. Concentration of alkoxysilane solutions should be kept low enough to avoid polymerization. Weak acid was sometimes used to accelerate the reaction between the hydroxylated surface and alkoxysilanes [222, 223]. Solutions with concentrations of GPTMS and ODTMS as 2 % (v/v) were modified with acetic acid in different percentages ranging from 0.4 % to 5 % (v/v) for optimization. 2 % was determined to be the optimal concentration, while the solution with less acid leaked out of the coating capillary causing cross-contamination. The solution with more than 2 % acid was corrosive to the AONP-modified surfaces. The reaction between APTMS and the modified MCs was very fast when the APTMS solution was capillary coated, so no catalyst was used.

Figure 23 shows the effect of the immersion time of AONP-modified MC in the alkoxysilane solutions. Two MCAs were prepared by immersing different MCs in the same 2 % solution of GPTMS and ODTMS, respectively, for different time periods. Under SEM, the MC surfaces appeared non-homogeneous when they were immersed for 6 h or longer. The two MCAs were exposed to hexane and ethanol samples and accordingly the obtained response profiles were compared. For the GPTMS-functionalized array, the MC functionalized for 2 h gave a much larger response than the one functionalized for 4 h. For the ODTMS-functionalized array, the hexane response increased with immersion time. The MC functionalized for 4 h gave the smallest response to ethanol, which may mean the phase surface had been

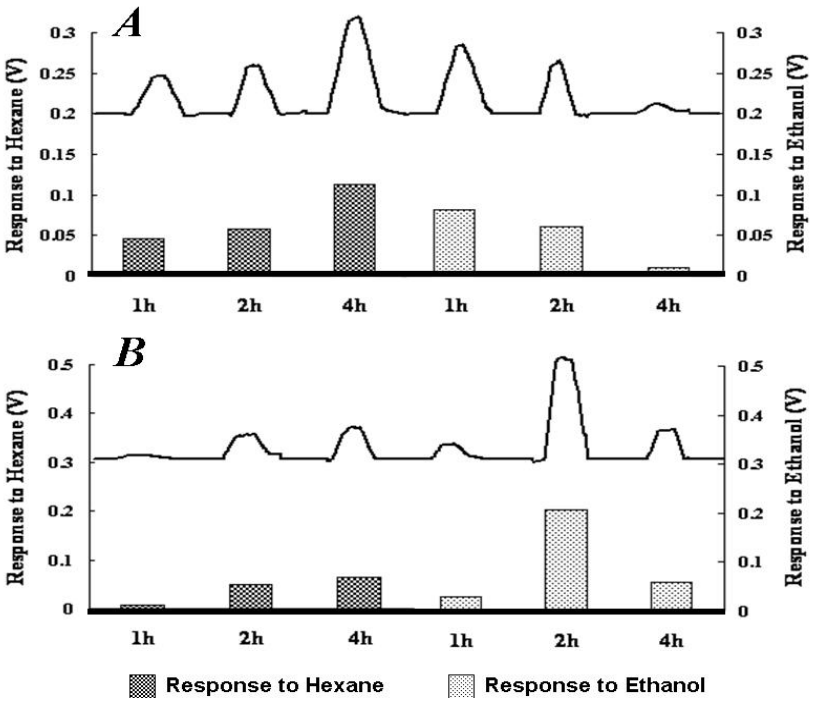

Figure 23. Response magnitude and associated profiles of AONP-nanostructured MCAs on exposure to 10 % hexane and 20 % ethanol diluted with nitrogen. The array was prepared by immersing three MCs in 2 % alkoxysilane (A: ODTMS, B: GPTMS) solution filled in capillarie for 1 h, 2 h and 4 h, respectively.

sufficiently functionalized and is very hydrophobic. For APTMS, no immersion time study was performed, due to the high reacting rate. The concentration of APTMS solution was optimized, ranging from 0.1 % (v/v) to 2 % (v/v). However, agglomerates appeared on the MC surface around 10 minute after capillary coating started, and was not dependent on the APTMS solution concentration. Consequently, 7 minute was picked as the immersion time. The nanostructured appearance was well retained after being functionalized with each alkoxysilane, which demonstrates the high stability of this new aluminium oxide phase in a liquid environment with no polymerization occurring on the surface. Figure 22H shows the SEM images of modified MC surface functionalized with GPTMS in the optimal manner. The image was obtained in secondary electron detection mode to reduce charge build-up for higher resolution.

5.3.3 Selectivity and Sensitivity

For VOC sensing, the MCA invokes different modes of interactions with the analytes, e.g. van der Waals, H-bonding, and π-π interactions. Figure 24 demonstrates the diversity of responses of the array to the four VOCs. There are primarily dispersive and induction interactions between hexane and the array (Figure 25A), with the former playing the dominating role, which most likely led to the largest deflection of the lever functionalized with ODTMS. H-bonding could form among hydroxyl groups, amino groups and glycidyloxy groups, which may explain why levers functionalized with APTMS and GPTMS responded to ethanol and aniline with a much bigger signal than the lever functionalized with ODTMS. The glycidyloxy group can act as donator of lone pairs to form H-bonding (Figure 25B) but the amino group may act as both

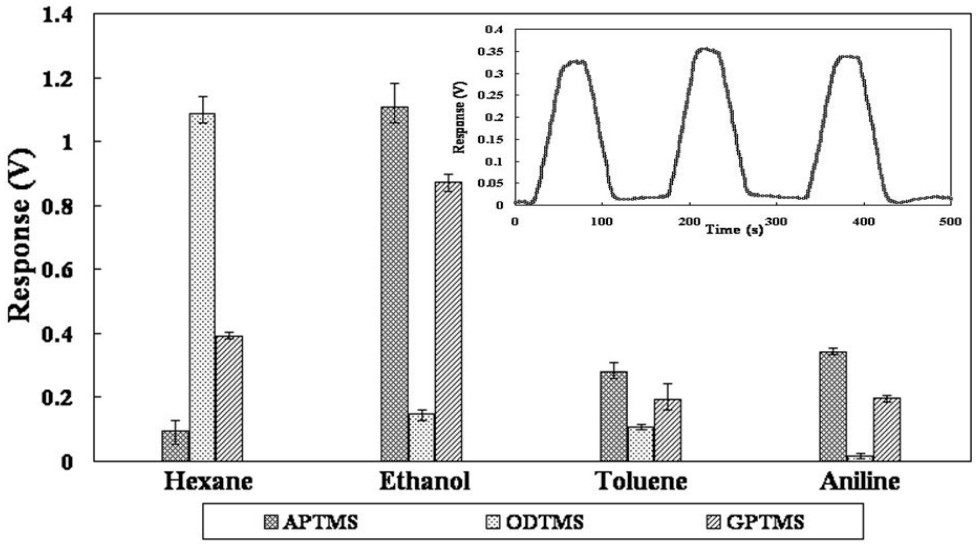

Figure 24. Selectivity plots demonstrate the response diversity to each headspace vapor for the MCA. In these experiments, each headspace vapor was injected for 60 second in triplicate and the peak signals were then averaged and plotted. A representative response profile of ODTMS-functionalized MC to 25 % hexane diluted in nitrogen is shown by the inset.

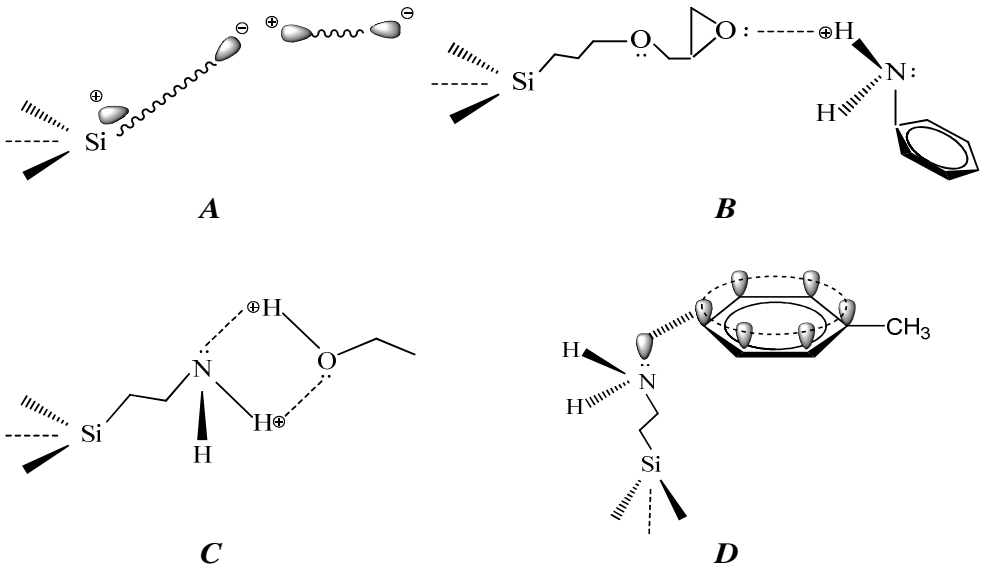

Figure 25. Representative conceptual diagram: (A) dispersive and induction interactions between hexane and octadecyl group in ODTMS, (B) H-bonding between aniline and glycidyloxy group in GPTMS, (C) H-bonding between ethanol and amino group in APTMS, (D) π-π interaction between toluene and amino group in APTMS.

donator and receptor (Figure 25C). Hence, the APTMS-functionalized MC can be expected to exhibit a greater diversity of interactions. Although toluene does not tend to H-bond, the delocalized π electrons of the benzene ring could overlap with the lone pairs of electrons of oxygen and nitrogen. The donation of lone pairs into the ring increases the density of π electrons [224] (Figure 25D), indicating toluene can interact more readily through π-π interaction with amino groups and glycidyloxy groups than octadecyl groups. As a result, the MCs functionalized with APTMS and GPTMS experienced more surface stress than those functionalized with ODTMS when exposed to toluene. Because the gaseous analytes have different vapor pressures, the response signals to different analytes are not comparable unless a S/C (signal:concentration) factor is applied. Hexane had the smallest S/C factor due to van der Waals forces which are often rather weak. S/C factor of toluene is smaller than ethanol and aniline because the π-π interaction is not expected to be as strong as H-bonding, while additional π-π interactions caused aniline to have a bigger S/C factor than ethanol.

The MCA was also capable of providing quantitative information by differentiating between varying concentrations of a given analyte. With analyte headspace diluted with nitrogen in different ratios, the response magnitude varied in a linear fashion (r-square value as high as 0.9962). This is demonstrated in Figure 26. The CVs in peak responses obtained from triplicate sample-injections were generally around 10 % (inset, Figure 24). Our prior work [162,163] has shown that the calibration plots were generally linear for 2 or more orders of magnitude while CVs for measurements using a given MC phase were generally 10 % or better. The array

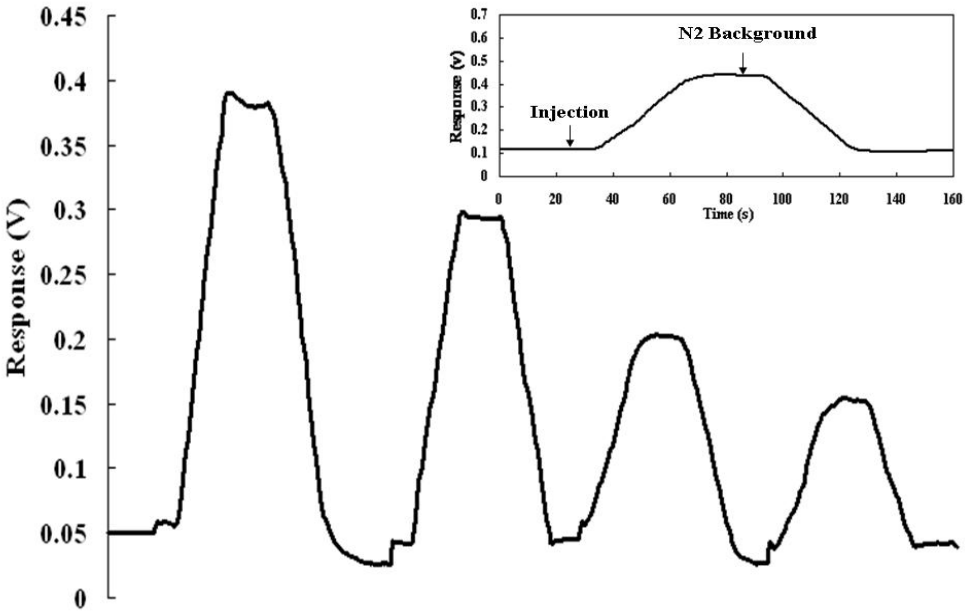

Figure 26. Representative response profile of MC functionalized with APTMS to aniline in order of decreasing sensor response at injected concentrations of 100 %, 75 %, 50 % and 25 % of the headspace vapor, respectively. The inset shows a representative entire response profile of one MC functionalized with ODTMS to 25 % hexane diluted in nitrogen. The arrows denote points of introducing hexane sample and nitrogen background in the flow cell, respectively.

demonstrated limits of detection as low as 0.13 μg/mL for aniline, based on 3σ of triplicate injections divided by the slope of the corresponding calibration plot.

Figure 27A shows the response profiles from a MCA in which two MCs were differentially functionalized with 0.5 mg/mL anti-hIgG and anti-biotin, respectively. Antibody-antigen interactions involving high specificity is a desirable characteristic for biosensors. We exploit the high affinity that is inherent to antibody-antigen binding. This provides our array with high selectivity and sensitivity. The MC functionalized with anti-IgG only responded to 0.05 mg/mL hIgG, while the MC functionalized with anti-biotin only responded to 0.05 mg/mL biotin, and no response was observed at all on exposure to 0.05 mg/mL BSA which was used as a non-specific protein. The functionalized MC started to deflect less than 1 min after the corresponding analyte was injected, which demonstrated a satisfactory sensitivity.

It is a base requirement of any true sensor that reversibility must be maintained while achieving high sensitivity and selectivity. Especially for biosensors, problems can arise from a potential lack of reversibility due to the high binding constants of bioaffinity reagents. In our previous work, we observed sensitive, reversible bio-nanomechanical responses [185, 216]. In a similar manner, it can be seen from Figure 27A that we observed reversible responses for antibody-AONP-modified MCs. The interplay between sensitivity, selectivity, and reversibility is interesting and under investigation by our group. Among the possible influencing factors are the complex effects of nano-confinement, chemical immobilization, and the fact that we expose the surfaces to sample for variable lengths of time but not to point of establishing

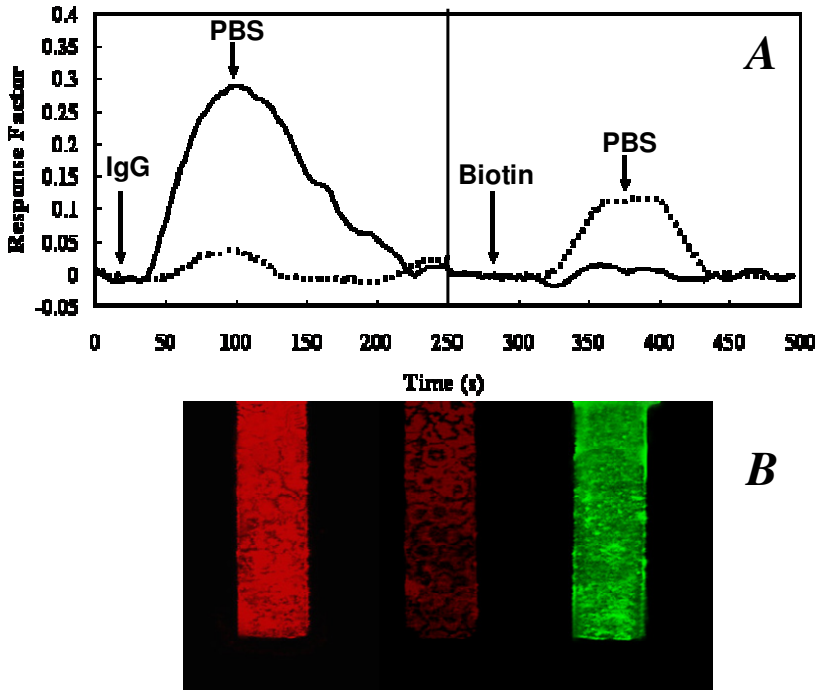

Figure 27. (A) Response profiles of AONP-fabricated MCs in the same array but differentially functionalized with 0.5 mg/mL anti-hIgG (solid line) and anti-biotin (dotted line) on exposure to 0.05 mg/mL hIgG (left) and 0.05 mg/mL biotin (right), respectively. The arrows denote points of introducing hIgG, biotin and PBS background in the flow cell, respectively. (B) Combined fluorescence microscopy images of differentially functionalized AONP-fabricated MCA: FITC labeled anti-IgG immobilized on the right lever was excited by 488 nm laser and Alexa 633 labeled anti-IgG immobilized on the left lever was excited by 633 nm laser.

equilibrium or saturation.

Furthermore, in order to validate the feasibility to successfully immobilize bio-receptors onto the AONP-modified MC surfaces through cross-linking with GA, with the same manner, another MCA was differentially functionalized with 0.5 mg/mL fluorescein isothiocyanate (FITC) labeled anti-bovine IgG and 0.5 mg/mL Alexa fluor 633 labeled goat anti-hIgG. Two fluorescence microscope images were taken by the Leica SP2 microscope, with the MCA excited by the 488 nm laser and the 633 nm laser one after the other (Figure 27B). Green color and red color were emitted on the FITC-labeled and Alexa fluor 633-labeled MC, respectively. The non-labeled MCs appeared very slightly red when excited by the 633 nm laser, which we believe is due to the auto-fluorescence of the aldehyde groups [225, 226].

5.3.4 Long-term and MC-to-MC Reproducibility

Response profiles for the six MCs in the VOC-sensing array were highly reproducible among replicate exposures to VOCs on the same day, and there was no distinct difference between the response pattern of the MCA collected initially and 4 weeks later. It should be noted that during that period of time the array was always kept in the flow cell even when it was not used. From our results, long-term MC response reproducibility is quite satisfactory. Good lever to lever reproducibility was observed between two duplicate MCs functionalized in the same manner, which demonstrates the uniformity of the AONP layer immobilized on the surface of the whole MCA chip. However, the array-to-array reproducibility was not satisfactory probably due to array-to-array variations of both size and lever stress, even though the

two arrays were modified with the same AONP slurry. It should be noted that the variation in resonance frequency for the commercial MCAs we purchased often varies by around 15 % in a given batch.

5.3.5 AONP-Modification and Enhanced Sensitivity

A MCA without being modified by AONP on the surface was functionalized with the three alkoxysilanes in the same optimized protocol. Although functionalized in the same manner, plain silicon MCs gave much smaller response signals than the AONP-nanostructured MCs. It should be noted that the silicon MCs were activated in boiled piranha solution before being functionalized so there should be an abundance of hydroxyl groups on the surface to react with alkoxysilanes like aluminium oxide. Hence, enhanced surface area with AONP-treatment should be the primary reason for such an obvious increase in response magnitude (in some case with a factor higher than 100 %), even considering the array-to-array variation in resonance frequency (only around 15 %).

In summary, we developed a novel method to modify MC surfaces with AONP. This creates a stable nanostructured MC with high surface area. We used commercially available metal oxide nano-particles to create a functional nanostructure for the future of MC sensing. This work explores in detail the potential of aluminium oxide and other metal oxides that can be functionalized with linker compounds as a sensing surface in the field of MC sensors by functionalizing the newly developed AONP-modified MCs with chemical or biological receptors for enhanced selectivity and sensitivity.

CHAPTER 6: CONCLUSION

In the field of MC-based sensing, great effort has been spent to achieve higher sensitivity and enhanced selectivity. MCs with increased surface areas are usually preferred for obtaining better sensitivity. Realistic sample analysis has introduced new challenges that necessitate the distributed specificity and selectivity of MC multi-sensor arrays. This dissertation work demonstrates the application of MCAs on the analysis of realistic gas-phase and liquid-phase analytes.

In the first two chapters, MCs and MCAs are introduced and their background is discussed. This background discussion includes the evolution and fabrication of MC sensors. Types of surface modification, operation modes, and detection schemes of MCs and MCAs are presented.

All of the MCAs utilized in this dissertation work were differentially functionalized after the cantilever's active surface was modified with nanostructured phases. Specific recognition phases were immobilized onto each individual lever so that the MCA could demonstrate distributed selectivity, with a distinct response pattern for each analyte. Moreover, for each MCA, the magnitude of response for each phase increased with the concentration of analyte in a linear fashion.

The first major division of this dissertation work focuses on preparing MCAs with previously developed nanostructured MCs and demonstrating their highly distributed selectivity. Chapter 3 discusses the detailed research of metal ion sensing with a MCA modified with gold nanostructured (DA) phase and subsequently functionalized using capillary coating. Different thiol ligands are immobilized onto the DA surface and then

each type of cation interacts with the MCA phases to generate a distinguishable response pattern. LOD as low as 10^{-7} M was derived from the calibration plots. Moreover, all metal cations were identified using SVM with some of the metals showing high prediction rates. Chapter 4 discusses the detection of landfill siloxane compounds with another gold nanostructured MCA coated with different RPs. The MCA incorporates several different interactions with the gas phase analyte. The cyclic siloxane produces a more distinguishable response pattern when compared to linear siloxanes, which demonstrated satisfactory recognition character of the array. LOD as low as 0.017 ppm was obtained, which is comparable with the more traditional GC-MS technique used for siloxane detection.

The second major division of this dissertation work focused on developing a new nanostructured MC sensor. This innovation involved chemically immobilizing AONP onto MC surfaces using TMOS as cross-linker, to generate a new stable and nanostructured platform for preparing MCAs. Optimization work was carried out on this new AONP phase to ensure good surface uniformity and high surface area. AONP-nanostructured MCs were subsequently differentially functionalized using capillary coating and immobilization of sensing sites was validated by FT-IR. One MCA was prepared for gas phase VOC sensing, which illustrated good sensitivity with a LOD as low as 0.13 μg/mL. Another ANOP-nanostructured MCA was prepared with two model biological proteins, to differentiate biological analytes in liquid phase. Both MCAs provided a distinctive response pattern for each specific analyte, showing that well-behaved MCAs can be created on this new AONP-nanostructured MC

platform.

In conclusion, the goal and major accomplishment of all the research presented in this work lies in developing MCAs which may be more applicable to realistic sample analysis. Contributing to MCA advancement helps further MC sensor technology for the future.

REFERENCES

1. Berger, R.; Lang, H.-P.; Gerber, Ch.; Gimzewski, J. K.; Fabian, J. H.; Scandella, L.; Meyer, E.; Guntherodt, H.-J. *Chem. Phys. Lett.,* **1998**, *294(4, 5),* 363-369.

2. Wachter, E. A.; Thundat, T. *Rev. Sci. Instrum.* **1995**, *66(6)*, 3662-3667.

3. Moulin, A. M.; Stephenson, R. J.; Welland, M. E. *J. Vac. Sci. Technol.* **1997**, *15(3),* 590-596.

4. Tuller, H. L.; Mlcak, R. *Curr. Opin. Solid State Mater. Sci.* **1998**, *3(5),* 501-504.

5. Datskos, P. G.; Sepaniak, M. J.; Tipple, C. A.; Lavrik, N. *Sens. Actuat. B-Chem.* **2001**, *76(1-3)*, 393-402.

6. Kovacs, G. T. A. *Micromachined Transducers*; McGraw-Hill: New York, 1998.

7. Thundat, T.; Oden, P. I.; Warmack, R. J. *Microscale Thermophys. Eng.* **1997**, *1(3)*, 185-199.

8. Berger, R.; Gerber, Ch.; Lang, H.-P.; Gimzewski, J. K. *Microelectron. Eng.* **1997**, *35*, 373-379.

9. Moulin, A. M.; O'Shea, S. J.; Welland, M. E. *Ultramicroscopy* **2000**, *82(1-4)*, 23-31.

10. Craighead, H. G. *Science* **2000**, *290(5496)*, 1532-1535.

11. Pereira, R. S. *Biochem. Pharmacol.* **2001**, *62(8)*, 975-983.

12. Sarid, D. *Scanning Force Microscopy*; Oxford University Press: New York, 1991.

13. Butt, H.-J. *J. Colloid Interface Sci.* **1996**, *180(1)*, 251-260.

14. Samuel, J.; Brinker, C. J.; Frink, L. J. D.; Van Swol, F. *Langmuir* **1998**, *14(10)*, 2602-2605.

15. Sader, J. E. J. *Appl. Phys*. **2002**, *91(11)*, 9354-9361.

16. Mamin, H. J.; Rugar, D. *Appl. Phys. Lett.* **2001**, *79(20)*, 3358-3360.

17. Datskos, P. G.; Thundat, T. *J. Nanosci. Nanotechnol.* **2002**, *2(3/4)*, 369-373.

18. Berger, R.; Gerber, Ch.; Gimzewski, J. K.; Meyer, E.; Guentherodt, H. J. *Appl. Phys. Lett.* **1996**, *69(1)*, 40-42.

19. Oden, P. I.; Datskos, P. G.; Thundat, T.; Warmack, R. J. *Appl. Phys. Lett.* **1996**, *69(21)*, 3277-3279.

20. Cleland, A. N. *Nature* **2004**, *431(7006)*, 251-252.

21. Lavrik, N. V.; Datskos, P. G. *Appl. Phys. Lett.* **2003**, *82(16)*, 2697-2699.

22. Timoshenko, S. *Theory of Plates and Shells*, McGraw-Hill: New York, 1940.

23. Stoney, G. G. *Proc. R. Soc. London, Ser.* **1909**, *82*, 172.

24. Norton, J. *U. S. Patent No.2* **1943***, 307*, 800.

25. Shaver, P. J. *Rev. Sci. Instrum.* **1969**, *40(7)*, 901-905.

26. Kuhn, W.; Hargitay, B.; Katchalsky, A.; Eisenberg, H. *Nature* **1950**, *165*, 514-516.

27. Sussman, M. V.; Katchalsky, A. *Science* **1970**, *167(3914)*, 45-47.

28. Dahmen, K.; Lehwald, S.; Ibach, H. *Surf. Sci.* **2000**, *446(1-2)*, 161-173.

29. Jones, R. V. *Proc. R. Soc. London, Ser.* **1959**, *A 249*, 100.

30. Taylor, E. H.; Waggener, W. C. *J. Phys. Chem.***1979**, *83(10)*, 1361-1362.

31. Newell, W. E. *Science* **1968**, *161*, 1320.

32. Behm, R. J.; Hoesler, W.; Ritter, E.; Binnig, G. *Phys. Rev. Lett.* **1986**, *56(3)*, 228-231.

33. Karrasch, S.; Hegerl, R.; Hoh, J. H.; Baumeister, W.; Engel, A. *Proc. Natl. Acad. Sci.* **1994**, 91(3), 836-838.

34. Mueller, D. J.; Schabert, F. A.; Bueldt, G.; Engel, A. *Biophys. J.* **1995**, *68(5)*, 1681-1686.

35. Gimzewski, J. K.; Gerber, Ch.; Meyer, E.; Schlittler, R. R. *Chem. Phys. Lett.* **1994**, *217(5-6)*, 589-594.

36. Timoshenko, S. *Optical Soc. Am.* **1925**, *11*, 233-255.

37. Mason, R.; Jalbert, C. A.; O'Rourke Muisener, P. A. V.; Koberstein, J. T.; Elman, J. F.; Long, T. E.; Gunesin, B. Z. *Adv. Colloid Interface Sci.* **2001**, *94(1-3)*, 1-19.

38. Martinez, R. E.; Augustyniak, W. M.; Golovchenko, J. A. *Phys. Rev. Lett.* **1990**, *64(9)*, 1035-1038.

39. Ibach, H. *J. Vac. Sci. Technol.* **1994**, *12*, 2240-2245.

40. Koch, R. *Appl. Phys. A: Mater. Sci. Process.* **1999**, *69(5)*, 529-536.

41. Shuttleworth, R. *Proc. Phys. Soc. London* **1950**, *63A*, 444-457.

42. Hazel, J. L.; Tsukruk, V. V. *J. Tribol.* **1998**, *120(4)*, 814-819.

43. Klein, C. A. *J. Appl. Phys.* **2000**, *88(9)*, 5487-5489.

44. Thundat, T.; Warmack, R. J.; Chen, G. Y.; Allison, D. P. *Appl. Phys. Lett.* **1994**, *64(21)*, 2894-2896.

45. Braun, T.; Barwich, V.; Ghatkesar, M. K.; Bredekamp, A. H.; Gerber, C.; Hegner, M.; Lang, H.-P. *Phys. Rev. E* **2005**, *72(3-1)*, 031907/1-031907/9.

46. McFarland, A. W.; Poggi, M. A.; Bottomley, L. A.; Colton, J. S. *J. Micromech. Microeng.* **2005**, *15*, 785.

47. Meyer, G.; Amer, N. M. *Appl. Phys. Lett.* **1988**, *53*, 1045.

48. Lang, H.-P.; Hegner, M.; Gerber, C. *Mater. Today* 2005, *8*, 30-36.

49. Shekhawat, G.; Tark, S. H.; Dravid, V. P. *Science* **2006**, *311*, 1592-1595.

50. Bottomley, L. A.; Poggi, M. A.; Shen, S. X. *Anal. Chem.* **2004**, *76*, 5685-5689.

51. Helm, M.; Servant, J. J.; Saurenbach, F.; Berger, R. *Appl. Phys. Lett.* **2005**, *87*, 064101/1- 064101/3.

52. Rugar, D.; Mamin, H. J.; Guethner, P. *Appl. Phys. Lett.* **1989**, *55*, 2588-2590.

53. Adams, J. D.; Rogers, B.; Manning, L.; Hu, Z.; Thundat, T.; Cavazos, H.; Minne, S. C. *Sens. Actuat. A-Phys.* **2005**, *121*, 457-461.

54. Britton, C. L.; Jones, R. L.; Oden, P. I.; Hu, Z.; Warmack, R. J.; Smith, S. F.; Bryan, W. L.; Rochelle, J. M. *Ultramicroscopy* **2000**, *82(1-4)*, 17-21.

55. Amantea, R.; Knoedler, C. M.; Pantuso, F. P.; Patel, V. K.; Sauer, D. J.; Tower, J. R. *Proc. SPIE-Int. Soc. Opt. Eng.* **1997**, *3061*, 210-222.

56. Buehler, J.; Steiner, F.-P.; Baltes, H. *J. Micromech. Microeng.* **1997**, *7(1)*, R1-R13.

57. Hierlemann, A.; Brand, O.; Hagleitner, C.; Baltes, H. *Proc. IEEE* **2003**, *91*, 839-863.

58. Johansson, A.; Calleja, M.; Ramussen, P. A.; Biosen, A. *Sens. Actuat. B-Chem.*

2005, *123–124*, 111.

59. Calleja, M.; Nordstorm, M.; Alvarez, M.; Tamayo, J.; Lechuga, L. M.; Biosen, A. *Ultramicroscopy* **2005**, *105*, 215-222.

60. Datskos, P. G.; Sauers, I. *Sens. Actuat. B-Chem.* **1999**, *61*, 75-82.

61. Berger, R.; Delamarche, E.; Lang, H.-P.; Gerber, C.; Gimzewski, J. K.; Meyer, E.; Guntherodt, H. J. *Appl. Phys. A: Mater. Sci. Process.* **1998**, *66*, S55-S59.

62. Pinnaduwage, L. A.; Boiadjiev, V.; Hawk, J. E.; Thudat, T. *Appl. Phys. Lett.* **2003**, *83*, 1471-1473.

63. Kaneko, D.; Gong, J. P.; Osada, Y. *J. Mater. Chem.* **2002**, *12*, 2169-2177.

64. Boisen, A.; Thaysen, J.; Jensenius, H.; Hansen, O. *Ultramicroscopy* **2000**, *82*, 11-16.

65. Zhao, Q.; Zhu, Q.; Shih, W. Y.; Shih, W.-H. *Sens. Actuat. B-Chem.* **2006**, *117*, 74-79.

66. Kadam, A.; Nordin, G. P.; George, M. A.; *J. Vac. Sci. Technol. B* **2006**, *24*, 2271-2275.

67. Yang, Y.; Ji, H.-F., Thundat, T. *J. Am. Chem. Soc.* **2003**, *125*, 1124-1125.

68. Baughman, R. H.; Cui, C. X.; Zakhidov, A. A.; Iqbal, Z.; Barisci, J. N.; Spinks, G. M.; Wallace, G. G.; Mazzoldi, A.; De Rossi, D.; Rinzler, A. G.; Jaschinski, O.; Roth, S.; Kertesz, M.; *Science* **1999**, *284*, 1340-1344.

69. Lavrik, N. V.; Tipple, C. A.; Sepaniak, M. J.; Datskos, P. G.; *Biomed. Microdevices* **2001**, *3*, 35-44.

70. Amirola, J.; Rodriguez, A.; Casaner, L.; Santos, J. P.; Gutierrez, J.; Horrillo, M. C. *Sens. Actuat. B-Chem.* **2005**, *111–112*, 247-253.

71. Betts, T. A.; Tipple, C. A.; Sepaniak, M. J.; Datskos, P. G.; *Anal. Chim. Acta* **2000**, *422*, 89-99.

72. Baller, M. K.; Lang, H.-P.; Fritz, J.; Gerber, C.; Gimzewski, J. K.; Drechsler, U.; Rothuizen, H.; Despont, M.; Vettinger, P.; Battiston, F. M.; Ramseyer, J. P.; Fornaro, P.; Meyer, E.; Guntherodt, H.-J.; *Ultramicroscopy* **2000**, *82*, 1-9.

73. Zhang, Y.; Ji, H.-F.; Brown, G. M.; Thundat, T. *Anal. Chem.* **2003**, *75*, 4773-4777.

74. Then, D.; Vidic, A.; Ziegler, C. *Sens. Actuat. B-Chem.* **2006**, *117*, 1-9.

75. Bumbu, G.-G.; Kircher, G.; Wolkenhauer, M.; Berger, R.; Gutmann, J. S. *Macromol. Chem. Phys.* **2004**, *205*, 1713-1720.

76. Battiston, F. M.; Ramseyer, J.-P.; Lang, H.-P.; Baller, M. K.; Gerber, C.; Gimzewski, J. K.; Meyer, E.; Guntherodt, H.-J. *Sens. Actuat. B-Chem.* **2001**, *77*, 122-131.

77. Kim, B. H.; Prins, F. E.; Kern, D. P.; Raible, S.; Weimer, U. *Sens. Actuat.B-Chem.* **2001**, *78*, 12-18.

78. Li, M.; Tang, H. X.; Roukes, M. L. *Nat. Nanotechnol.* **2007**, *2*, 114-120.

79. Bietsch, A.; Zhang, J.; Hegner, M.; Lang, H.-P.; Gerber, C. *Nanotechnology* **2004**, *15*, 873-880.

80. Lochon, F.; Fadel, L.; Dufour, I.; Rebiere, D.; Pistre, J. *Mater. Sci. Eng. C* **2006**, *26*, 348-353.

81. Zhao, J.; Berger, R.; Gutmann, J. S. *Appl. Phys. Lett.* **2006**, *89*, 033110/1-033110/3.

82. LeMieux, M. C.; McConney, M. E.; Lin, Y. H.; Singamaneni, S.; Jiang, H.; Bunning, T. J.; Tsukruk, V. V. *Nano Lett.* **2006**, *6*, 730-734.

83. Abu-Lail, N. I.; Kaholek, M.; LaMattina, B.; Clark, R. L.; Zauscher, S. *Sens. Actuat. B-Chem.* **2006**, *114*, 371-378.

84. Bashir, R.; Hilt, J. Z.; Eilbol, O.; Gupta, A.; Peppas, N. A. *Appl. Phys. Lett.* **2002**, *81*, 3091-3093.

85. Lin, Y. H.; McConney, M. E.; LeMieux, M. C.; Peleshanko, S.; Jiang, C.; Singamaneni, S.; Tsukruk, V. V. *Adv. Mater.* **2006**, *18*, 1157-1161.

86. Pinnaduwage, L. A.; Thundat, T.; Hawk, J. E.; Hedden, D. L.; Britt, P. F.; Houser, E. J.; Stepnowski, S.; McGill, R. A.; Bubb, D. *Sens. Actuat.B-Chem.* **2004**, *99*, 223-229.

87. Comini, E.; Faglia, G.; Sberveglieri, G. *Sens. Actuat. B-Chem.* **2001**, *76*, 270-274.

88. Winquist, F.; Holmin, S.; Krantz-Rulcker, C.; Wide, P.; Lundstorm, I. *Anal. Chim. Acta* **2000**, *406*, 147-157.

89. Porter, T. L.; Eastman, M. P.; Macomber, C; Delinger, W. G.; Zhine, R. *Ultramicroscopy*, **2003**, *97*, 365-369.

90. Kalchenko, V. I.; Koshets, I. A.; Matsas, E. P.; Kopylov, O. N.; Solovyov, A.;

Kazantseva, Z. I.; Shirshov, Y. M. *Mater. Sci.* **2002**, *20*, 73-88.

91. LIoyd-Spetz, A.; Tobias, P.; Uneus, L.; Svenningstorp, H.; Ekedahl, L.-G.; Lundstorm, I. *Sens. Actuat. B-Chem.* **2000**, *70*, 67-76.

92. Penza, M.; Cassano, G.; Tortorella, F. *Meas. Sci. Technol.* **2002**, *13*, 846-858.

93. Calleja, M.; Tamayo, J.; Johansson, A.; Rasmussen, P.; Lechuga, L. M.; Boisen, A. *Sens. Lett.* **2003**, *1*, 20-24.

94. Maute, M.; Raible, S.; Prins, F. E.; Kern, D. P.; Ulmer, H.; Weimar, U.; Gopel, W. *Sens. Actuat. B-Chem.* **1999**, *58*, 505-511.

95. Wu, S.-Y.; Berkenbosch, R.; Lui, A.; Green, J.-B. D. *Analyst* **2006**, *131*, 1213-1215.

96. Zou, J.; Bullen, D.; Wang, X.; Liu, C.; Mirkin, C. A. *Appl. Phys. Lett.* **2003**, *83*, 581-583.

97. Banerjee, D. *BioMEMS Biomed. Nanotechnol.* **2006**, *1*, 265-305.

98. Zhang, J.; Lang, H.-P.; Huber, F.; Bietsch, A.; Grange, W.; Certa, U.; McKendry, R.; Guntherodt, H. J.; Hegner, M.; Gerber, C. *Nature Nanotechnol.* **2006**, *1*, 214-220.

99. McKendry, R.; Zhang, J.; Arntz, Y.; Strunz, T.; Hegner, M.; Lang, H.-P.; Baller, M. K.; Certa, U.; Meyer, E.; Guntherodt, H.-J.; Gerber, C. *Proc. Natl. Acad. Sci.* **2002**, *99*, 9783-9788.

100. Jutten, C., Herault, J.; Comon, P.; Sorouchiary, E.; *Signal Process.* **1991**, *24*, 1-29.

101. Comon, P. *Signal Process.* **1994**, *36 (3)*, 287-314.

102. Bell, A. J.; Sejnowski, T. J.; *Vis. Res.* **1997**, *37 (23)*, 3327-3338.

103. Makeig, S.; Debener, S.; Onton, J.; Delorme, A. *Trends Cogn. Sci.***2004**, *8 (5)*, 204-210.

104. Carrascosa, L. G.; Moreno, M.; Alvarez, M.; Lechuga, L. M. *TrAC Trends Anal. Chem.* **2006**, *25*, 196-206.

105. Raiteri, R.; Grattarola, M.; Butt, H. J.; Skladal, P. *Sens. Actuat. B-Chem.* **2001**, *B79*, 115-126.

106. Datskos, P. G.; Lavrik, N. V.; Sepaniak, M. J. *Intro. Nanoscale Sci. Technol.* **2004**, 417-439.

107. Lavrik, N. V.; Sepaniak, M. J.; Datskos, P. G. *Rev. Sci. Instrum.* **2004**, *75*, 2229-2253.

108. Lang, H.-P.; Hegner, M.; Meyer, E.; Gerber, C. *Nanotechnology* **2002**, *13*, R29-R36.

109. Karnati, C.; Dua, H.; Ji, H.-F.; Xua, X.; Lvov, Y.; Mulchandani, A.; Mulchandani, P.; Chen, W. *Biosens. Bioelectron.* **2007**, *22*, 2636-2642.

110. Long, Z.; Storey, J.; Lewis S.; Sepaniak, M. J. *Anal. Chem.* **2009**, *81* (7), 2575–2580

111. Chapman, P.; Long, Z.; Datskos, P. G.; Archibald, R.; Sepaniak, M. J. *Anal. Chem.* **2007**, *79* (18), 7062–7068.

112. Gfeller, K. Y.; Nugaeva, N.; Hegner, M. *Appl. Environ. Microbiol.* **2005**, *71*, 2626-2631.

113. Gfeller, K. Y.; Nugaeva, N.; Hegner, M. *Biosens. Bioelectron.* **2005**, *21*, 528-533.

114. Nugaeva, N.; Gfeller, K. Y.; Backmann, N.; Lang, H.-P.; Dueggelin, M.; Hegner, M. *Biosens. Bioelectron.* **2005**, *21*, 849-856.

115. Fritz, J.; Baller, M. K.; Lang, H.-P.; Rothuizen, H. V. P.; Meyer, E.; Guntherodt, H.-J.; Gerber, C.; Gimzewski, J. K. *Science* **2000**, *288*, 316-318.

116. Singamaneni, S; LeMieux, M. C.; Lang, H.-P.; Gerber C.; Lam, Y.; Zauscher, S.; Datskos, P. G.; Lavrik, N. V.; Jiang, H.; Naik, R. R.; Bunning, T. J.; Tsukruk, V. V. *Adv. Mater.* **2008**, *20*, 653–680.

117. Goeders, K. M.; Colton, J. S.; Bottomley, L. A. *Chem. Rev.* **2008**, *108*, 522-542.

118. Chang L. W. *Toxicology of metals*. Boca Raton: Lewis Publishers, 1996.

119. Rottmann, L.; Heumann, K. G. *Anal. Chem.* **1994**, *66*, 3709-3715.

120. Altenau, A. G.; Rogers, L. B. *Anal. Chem.* **1964**, *36*, 1726-1735.

121. Sutton, K.; Sutton, R. M. C.; Caruso, J. A. *J. Chromatogr. A* **1997**, *789*, 85-126.

122. Kang, S. W.; Park, C. M.; Cho, K. H.; Han, H. S. *Bull. Korean Chem. Soc.* **1993**, *14*, 59-62.

123. Janssen, L. J. J.; Koene, L. *Chem. Eng. J.* **2002**, *85*, 137-146.

124. Bakker, E. *Anal. Chim. Acta* **1997**, *350*, 329-340.

125. Hill, S. J.; Arowolo, T. A.; Butler, O. T.; Chenery, S. R. N.; Cook, J. M.; Cressar, M. S.; Miles, D. L. *J. Anal. At. Spectrom.* **2002**, *17*, 284-317.

126. Sarkar, M.; Das, M.; Datta, P. K. *J. Colloid Interface Sci.* **2002**, *246*, 263-269.

127. Babu, T. S.; Marder, J. B.; Tripuranthakam, S.; Dixon, D. G.; Greenberg, B. M. *Environ. Toxicol. Chem.* **2001**, *20*, 1351-1358.

128. Starodub, N. F.; Kanjuk, N. I.; Kukla, A. L.; Shirshov, Y. M. *Anal. Chim. Acta* **1999**, *385*, 461-466.

129. Blake, D. A.; Jones, R. M.; Blake, R. C.; Pavlov, A. R.; Darwish, I. A.; Yu, H. N. *Biosens. Bioelectron.* **2001**, *16*, 799-809.

130. Sepaniak, M. J.; Datskos, P. G.; Lavrik, N. V.; Tipple, C. A. *Anal. Chem.* **2002**, *74*, 568A-575A.

131. Dutta, P.; Chapman, P.; Datskos, P. G.; Sepaniak, M. J. *Anal. Chem.* **2005**, *77*, 6601-6608.

132. Lavrik, N. V.; Tipple, C.; Datskos, P. G.; Sepaniak, M.J. *Chem. Phys. Lett.* **2001**, 336, 371-376.

133. Dejesus, M. A.; Giesfeldt, K. S.; Sepaniak, M. J. *Appl. Spec.* **2003**, *57*, 428-438.

134. Archibald, R.; Datskos, P. G.; Devault, G.; Lamberti, V.; Lavrik, N. V.; Noid, D.; Sepaniak, M. J.; Dutta, P. *Anal. Chim. Acta* **2007**, *584* 101-105.

135. Senesac, L.; Dutta, P.; Datskos, P. G.; Sepaniak, M. J. *Anal. Chim. Acta* **2006**, *558*, 94-101.

136. Cortes C.; Vapnik, V. N. *Support Vector Networks, Machine Learning*, **1995**, *20*, 273-297.

137. Vapnik, V. N. *Statistical Learning Theory.* Wiley: New York, 1998.

138. Widrig, C. A.; Chung, C.; Porter, M. D. *J. Electroanal. Chem.* **1991**, *310,* 335.

139. Jia, C. R.; Batterman, S.; Godwin, C. *Atmos. Environ.* **2008**, *42(9)*, 2083-2100.

140. Lazar, L.; Balasanian, I.; Bandrabur, F. *Environ. Eng. Manage. J.* **2007**, *6(6)*, 529-535.

141. Potkay, J. A.; Lambertus, G. R.; Sacks, R. D.; Wise, K. D. *J. Microelectromech. S.* **2007**, *16(5)*, 1071-1079.

142. Kumar, A.; Sun, S. S.; Lees, A. J. *Coord. Chem. Rev.* **2008**, *252(8+9)*, 922-939.

143. Rizzo, S.; Sannicolo, F.; Benincori, T.; Schiavon, G.; Zecchin, S.; Zotti, Gi. *J. Mater. Chem.* **2004**, *14(12)*, 1804-1811.

144. James, D.; Scott, S. M.; Ali, Z.; O'Hare, W. T. *Microchim. Acta* **2005**, *149(1-2)*, 1-17.

145. Grate, J. W. *Chem. Rev.* **2000**, *100(7)*, 2627-2647.

146. Feng, L. D.; Huang, X. J.; Choi, Y. K. *Microchim. Acta* **2007**, *156(3-4)*, 245-251.

147. Miller, J. P. *J. Chemom.* **2007**, *20(1-2)*, 34-42.

148. Norden, B.; Broberg, P.; Lindberg, C.; Plymoth, A. *Chem. Biodiversity.* **2005**, *2(11)*, 1487-1494.

149. Eiceman, G. A.; Wang, M.; Prasad, S.; Schmidt, H.; Tadjimukhamedov, F. K.; Lavine, B. K.; Mirjankar, N. *Anal. Chim. Acta* **2006**, *579(1)*, 1-10.

150. Chapman, P. J.; Long, Z.; Datskos, P. G.; Archibald, R.; Sepaniak, M. J. *Anal. Chem.* **2007**, *79*, 7062-7068.

151. Senesac, L. R.; Dutta, P.; Datskos, P. G.; Sepaniak, M. J. *Anal. Chim. Acta* **2006**, *558(1-2)*, 94-101.

152. Lombardi, L.; Carnevale, E.; Corti, A. *Energy* **2006**, *31(15)*, 3208-3219.

153. Kjeldsen, P.; Fischer, E. V. *Waste Manage. Res.* **1995**, *13(5)*, 467-484.

154. Kumar, D.; Alappat, B. J. *Clean Technol. Environ. Policy* **2005**, *7(3)*, 190-197.

155. Dolgen, D.; Sarptas, H.; Alpaslan, N.; Kucukgul, O. *Energy Sources* **2005**, *27(15)*, 1483-1492.

156. Accettola, F.; Guebitz, G. M.; Schoeftner, R. *Clean Technol. Environ. Policy* **2008**, *10(2)*, 211-218.

157. Thorneby, L.; Mathiasson, L.; Martensson, L.; Hogland, W. *Waste Manage. Res.* **2006**, *24*, 183-194.

158. Mathison, S.; McCaw, K.; Lewis, R.; Magers, K.; Lee, J. *Water Environment Laboratory Solutions* **2005**, *12(5)*, 6-11.

159. Guan, S. *Anal. Chem.* **2003**, *75*, 4551-4557.

160. Penza, M.; Cassano, G. *Sens. Actuat. B-Chem.* **2003**, *89(3)*, 269-284.

161. Thundat, T.; Oden, P. I.; Warmack, R. J. *Proc.-Electrochem. Soc.* **1997**, *97-5*, 179-187.

162. Lavrik, N. V.; Tipple, C. A.; Sepaniak, M. J.; Datskos, P. G. *Chem. Phys. Lett.* **2001**, *336*, 371-376.

163. Tipple, C. A.; Lavrik, N. V.; Culha, M.; Headrick, J.; Datskos, P.; Sepaniak, M. J. *Anal. Chem.* **2002**, *74*, 3118-3126.

164. Dutta, P.; Chapman, P. J.; Datskos, P. G.; Sepaniak, M. J. *Anal. Chem.* **2005**, *77(20)*, 6601-6608.

165. Baker, G. A.; Desikan, R.; Thundat, T. *Anal. Chem.* **2008**, *80*, 4860–4865.

166. Pinnaduwage, L. A.; Thundat, T.; Hawk, J. E.; Hedden, D. L.; Britt, P. F.; Houser, E. J.; Stepnowski, S.; McGill, R. A.; Bubb, D. *Sens. Actuat. B-Chem.* **2004**, *99(2-3)*, 223-229.

167. Porter, T. L.; Vail, T. L.; Eastman, M. P.; Stewart, R.; Reed, J.; Venedam, R.; Delinger, W. *Sens. Actuat. B-Chem.* **2007**, *123(1)*, 313-317.

168. Adams, J. D.; Parrott, G.; Bauer, C.; Sant, T.; Manning, L.; Jones, M.; Rogers, B.; McCorkle, D.; Ferrell, T. L. *Appl. Phys. Lett.* **2003**, *83(16)*, 3428-3430.

169. Dutta, P.; Senesac, L. R.; Lavrik, N. V.; Datskos, P. G.; Sepaniak, M. J. *Sens. Lett.* **2004**, *2(3, 4)*, 238-245.

170. Tortajada-Genaro, L. A.; Campins-Falco, P.; Blasco-Gomez, F.; Bosch-Reig, F. *Analyst* **2000**, *125(4)*, 771-782.

171. Nepote, A. J.; Olivieri, A. C. *Anal. Chim. Acta* **2001**, *439(1)*, 87-94.

172. Reid, R. C.; Prausnitz, J. M.; Sherwood, T. K. *The properties of gases and liquids*, 4th ed.; McGraw-Hill: New York**,** 1987.

173. Poling, B. E.; Prausnitz, J. M.; O'Connell, J. P. *The properties of gases and liquids*, 5th ed.; McGraw-Hill: New York**,** 2001.

174. Olson, J. D. *Fluid Phase Equilib.* **1998**, *150*, 713-720.

175. Guo, Y. S.; Zhong, J.; Xing, Y.; Li, D.; Lin, R. S. *Energy Fuels* **2007**, *21(2)*, 1188-1192.

176. Yuan, W.; Hansen, A. C.; Zhang, Q. *Fuel* **2005**, *84(7-8)*, 943-950.

177. Flaningam, O. L. *J. Chem. Eng. Data* **1986**, *31(3)*, 266-272.

178. Harris, D. C. *Quantitative Chemical Analysis*, 7th ed.; W. H. Freeman: New York, 2006.

179. Chapman, P. J.; Dutta, P.; Datskos, P. G.; Devault, G. L.; Sepaniak, M. J. *Anal. Chem*. **2007**, *79*, 364-370**.**

180. Archbald, R.; Datskos, P. G.; Devault, G. L.; Lamberti, V.; Lavrik, N. V.; Noid, D.; Dutta, P.; Sepaniak, M. J. *Anal. Chim. Acta* **2007**, *584*, 101-105.

181. Herdin, G. R.; Gruber, F.; Kuffmeier, R.; Brandt, A. *ICE (Am. Soc. Mech. Eng.)* **2000**, *34 (3)*, 101-110.

182. Ajhar, M.; Melin, T. *Desalination* **2006**, *200(1-3)*, 234-235.

183. Ji, H.-F.; Thundat, T.; Dabestani, R.; Brown, G. M.; Britt, P. F.; Bonnesen, P. V. *Anal. Chem.* **2001**, *73(7),* 1572-1576.

184. Datskos, P. G.; Lavrik, N. V.; Sepaniak, M. J. *Sens. Lett.* **2003**, *1(1)*, 25-32.

185. Dutta, P.; Hill, K.; Datskos, P. G.; Sepaniak, M. J. *Lab Chip* **2007**, *7(9)*, 1184-1191.

186. Ji, H.-F.; Gao, H.; Buchapudi, K. R.; Yang, X.; Xu, X.; Schulte, M. K. *Analyst* **2008**, *133(4)*, 434-443.

187. Passian, A.; Protopopescu, V.; Thundat, T. *J. Appl. Phys.* **2006**, *100(11)*, 114314/1-114314/4.

188. Chen, Q.; Fang, J.; Ji, H.-F.; Varahramyan, K. *Microsyst. Technol.* **2008**, *14(6)*, 739-746.

189. Morshed, S.; Baldwin, K. E.; Zhou, B.; Prorok, B. C. *Sens. Lett.* **2009**, *7(1)*, 38-41.

190. Ansari, M. Z.; Cho, C. *Sensors* **2008**, *8(11)*, 7530-7544.

191. Park, J. H.; Kwon, T. Y.; Yoon, D. S.; Kim, H.; Kim, T. S. *Adv. Funct. Mater.* **2005**, *15(12)*, 2021-2028.

192. Zhang, X. R.; Xu, X. *Appl. Phys. Lett.* **2004**, *85(12)*, 2423-2425.

193. Raguse, B.; Mueller, K. H.; Wieczorek, L. *Adv. Mater.* **2003**, *15(11)*, 922-926.

194. Dohn, S.; Kjelstrup-Hansen, J.; Madsen, D. N.; Molhave, K.; Boggild, P. *Ultramicroscopy* **2005**, *105(1-4)*, 209-214.

195. Mertens, J.; Calleja, M.; Ramos, D.; Taryn, A.; Tamayo, J. *J. Appl. Phys.* **2007**, *101(3)*, 034904/1-034904/8.

196. Bergese, P.; Bontempi, E.; Chiari, M.; Colombi, P.; Damin, F.; Depero, L. E.; Oliviero, G.; Pirri, G.; Zucca, M. *Appl. Surf. Sci.* **2007**, *253(9)*, 4226-4231.

197. Lin, Y. H.; LeMieux, M. C.; McConney, M.; Tsukruk, V. V. *PMSE Preprints* **2006**, *94*, 845.

198. Leichle, T.; Silvan, M. M.; Belaubre, P.; Valsesia, A.; Ceccone, G.; Rossi, F.; Saya, D.; Pourciel, J. B.; Nicu, L.; Bergaud, C. *Nanotechnology* **2005**, *16(4)*, 525-531.

199. Coutrot, A. L.; Roblin, C.; Lafosse, X.; David, C.; Madouri, A.; Laloo, R.; Martrou, D. *Microelectron. Eng.* **2009**, *86(4-6)*, 1197-1199.

200. Stolyarova, S.; Cherian, S.; Raiteri, R.; Zeravik, J.; Skladal, P.; Nemirovsky, Y. *Sens. Actuat. B-Chem.* **2008**, *131(2)*, 509-515.

201. Tuller, H. L.; Mlcak, R. *J. Electroceram.* **2000**, *4(2/3)*, 415-425.

202. Tark, S. H.; Srivastava, A.; Chou, S.; Shekhawat, G.; Dravid, V. P. *Appl. Phys. Lett.* **2009**, *94(10)*, 104101/1-104101/3.

203. Lee, J. H.; Yoon, K. H.; Hwang, K. S.; Park, J.; Ahn, S.; Kim, T. S. *Biosens. Bioelectron.* **2004**, *20(2)*, 269-275.

204. Qazi, M.; Koley, G. *Sensors* **2008**, *8(11)*, 7144-7156.

205. Lee, J. H.; Hwang, K. S.; Park, J.; Yoon, K. H.; Yoon, D. S.; Kim, T. S. *Biosens. Bioelectron.* **2005**, *20(10)*, 2157-2162.

206. Lee, D.; Shin, N.; Lee, K. H.; Jeon, S. *Sens. Actuat. B-Chem.* **2009**, *137 (2)*, 561-565.

207. Kapa, P.; Pan, L.; Bandhanadham, A.; Fang, J.; Varahramyan, K.; Davis, W.; Ji, H.-F. *Sens. Actuat. B-Chem.* **2008**, *134 (2)*, 390-395.

208. Bhalerao, K. D.; Lee, S. C.; Soboyejo, W. O.; Soboyejo, A. B. O. *J. Mater. Sci.-Mater. M.* **2007**, *18(1)*, 3-8.

209. Capobianco, J. A.; Shih, W. Y.; Shih, W. H. *Rev. Sci. Instrum.* **2007**, *78(4)*, 046106/1-046106/3.

210. Capobianco, J. A.; Shih, W. Y.; Shih, W. H. *Rev. Sci. Instrum.* **2006**, *77(12)*, 125105/1-125105/6.

211. Cousin, P.; Smith, P. *J. Polym. Sci. Pol. Phys.* **1994**, *32(3)*, 459-468.

212. Duran, H.; Gitsas, A.; Floudas, G.; Mondeshki, M.; Steinhart, M.; Knoll, W. *Macromolecules* **2009**, *42 (8)*, 2881-2885.

213. Arntz, Y.; Seelig, J. D.; Lang, H.-P.; Zhang, J.; Hunziker, P.; Ramseyer, J. P.;

Meyer, E.; Hegner, M.; Gerber, Ch. *Nanotechnology* **2003**, *14(1)*, 86-90.

214. Zhang, J.; Lang, H. P.; Huber, F.; Bietsch, A.; Grange, W.; Certa, U.; McKendry, R.; Guntherodt, H. J.; Hegner, M.; Gerber, Ch. *Nat. Nanotechnol.* **2006**, *1(3)*, 214-220.

215. Dhayal, B.; Henne, W. A.; Doorneweerd, D. D.; Reifenberger, R. G.; Low, P. S. *J. Am. Chem. Soc.* **2006**, *128(11)*, 3716-3721.

216. Hill, K.; Dutta, P.; Zareba, A.; Eldridge, M. L.; Sepaniak, M. J. *Anal. Chim. Acta* **2008**, *625(1)*, 55-62.

217. Socrates, G. *Infrared and Raman Characteristic Group Frequencies*, 3rd ed.; John Wiley & Sons: West Sussex, England, 2001.

218. Ohno, K.; Mandai, Y.; Matsuura, H. *J. Mol. Struct.* **1992**, *268(1-3)*, 41-50.

219. Durig, J. R.; Beshir, W. B.; Godbey, S. E.; Hizer, T. J. *J. Raman Spectrosc.* **1989**, *20(5)*, 311-333.

220. Bernstein, H. J. *Spectrochim. Acta* **1962**, *18*, 161-170.

221. McKean, D. C.; Duncan, J. L.; Batt, L. *Spectrochim. Acta* **1973**, *29(6)*, 1037-1049.

222. Shmykov, A. Y.; Mjakin, S. V.; Vasiljeva, I. V.; Filippov, V. N.; Vylegzhanina, M. E.; Sukhanova, T. E.; Kurochkin, V. E. *Appl. Surf. Sci.* **2009**, *255(12)*, 6391-6396.

223. Cano-Serrano, E.; Blanco-Brieva, G.; Campos-Martin, J. M.; Fierro, J. L. G. *Langmuir* **2003**, *19(18)*, 7621-7627.

224. Raorane, D.; Lim, S. H.; Majumdar, A. *Nano Lett.* **2008**, *8(8)*, 2229-2235.

225. Baschong, W.; Suetterlin, R.; Laeng, R. H. *J. Histochem. Cytochem.* **2001**, *49(12)*, 1565-1571.

226. Werkmeister, J. A.; Tebb, T. A.; Peters, D. E.; Ramshaw, J. A. M. *Clin. Mater.* **1990**, *6(1)*, 13-20.

VITA

Zhou Long was born in Qingdao, China on March 8th, 1981. He was raised and went to grade school in Qingdao, China. He graduated junior high and high school from the No. 2 Middle School in Qingdao, China, in 1999. From there he went to Sichuan University in Chengdu, China, where he earned his B.S. in chemistry in 2003.

Zhou earned his doctorate in analytical chemistry at the University of Tennessee, Knoxville, TN in May of 2010. Upon graduation he will begin a job as a PhD Advanced Development Chemist.